CENTRO DE INVESTIGACIONES
EN OPTICA, A.C.

“DESIGN AND FABRICATION OF PHOTONIC COMPONENTS FOR TERAHERTZ FREQUENCIES”

Tesis que para obtener el grado de Doctor en Ciencias (Óptica)

Presenta: Mónica Ortiz Martínez

Director de Tesis: Dr. Enrique Castro Camus

León · Guanajuato · México

Mayo de 2021

Abstract

In this thesis we demonstrate numerically and experimentally four novel photonic devices for terahertz frequencies fabricated by three-dimensional printing. We present, to the best of our knowledge, the first 3D printed dielectric frequency filter for the terahertz band. The filter is formed by a dielectric diffractive grating printed over a rectangular waveguide of the same material. The operational principle consists in couple laterally an electromagnetic beam into the grating; if the exit angle of the diffracted mode is equal or greater than the total internal reflection angle inside the rectangular waveguide, the radiation will be confined and will propagate until it reaches the ends of the waveguide. For this study, we fabricated three different devices that filter 200 GHz, 250 GHz and 300 GHz depending on their physical dimensions. We also prove that these frequency filters can be tunable.

In addition, we demonstrate three innovative 3D printed devices that perform OR, AND, XOR logic operations at 130 GHz. The operation principle of these logic gates consist of two input electromagnetic waves that interfere to produce a desired output amplitude. The geometries of the Terahertz logic gates are formed by a combination of rectangular waveguides. Each device is evaluated for four input combinations: “on/on”, “on/off”, “off/on”

and “off/off”, where “on/off” means coupled/non-coupled radiation in each input. The output of these operations is the amplitude of the terahertz radiation at the end of the device. Upon comparing the numerical simulations with the experimental measurements, we achieved very similar results. This opens future possibilities to integrate these components in order to build more complex photonic circuits.

The four devices presented in this thesis were simulated using COMSOL Multiphysics and fabricated by Fusion Deposition Modeling. Subsequently, they were tested by terahertz time-domain spectroscopy. The results obtained in this thesis show that 3D printing technology is an efficient method to produce terahertz components that can be used in many areas such as telecommunication and for the fabrication of THz components for control and manipulation of THz waves.

A mi mamá Minerva y mi papá Eduardo
por su infinito amor e incondicional apoyo.

Acknowledgements

Firstly, I want to thank my advisor Dr. Enrique Castro Camus for the continuous support throughout this work, for his patience and for giving me the opportunity to learn about experimental physics and terahertz applications. Also, I would like to thank my country Mexico and CONACyT for the financial support throughout my degree. While the contributions presented in this thesis are mainly the result of my own work, science these days is a collaborative activity, therefore I would like to acknowledge the contribution of Arturo Hernandez Serrano, Manuel Justo Guerrero, Elodie Strupiechonski and Enrique Castro-Camus who took part in several aspects of the research presented here.

I want to thank my family: my parents, my sister Paloma and my brother Eduardo for constantly motivating me to do the things I love. Last but not least, I would like to thank my husband Oscar for so much love and for walking (and sometimes running) by my side in all my adventures.

Contents

Chapter 1

Introduction

Since long ago scientists have studied light and its properties [1, 2]. Until the middle of the seventeenth century, it was believed that light was formed by discrete particles called "corpuscles" that were emitted by sources such as the sun or the flame of a candle, which traveled in a straight line [3, 4]. In 1660 Huygens proved that the laws of optics could be explained based on the assumption that light had a wave nature. It was not until 1873 when a substantial discovery in the understanding of the nature of light occurred. This discovery was Maxwell's theoretical studies on electric and magnetic fields that allowed him to combine both in a single theory called electromagnetism [5, 6].

Nowadays, scientists continue studying the properties and applications of light. Depending on the frequency of the radiation it is possible to identify different areas of application. For instance, low frequencies ($10^5\,Hz - 10^{11}\,Hz$) are used in communication technologies, such as television, mobile phones and radios [7, 8]. High frequencies ($10^{15}\,Hz - 10^{22}$ Hz) such as visible

light or x-rays are commonly used in biomedical applications [7, 8]. Between low and high frequencies there exist a gap in the electromagnetic spectrum called the Terahertz-gap (10^{11} - 10^{13} Hz) [9, 10]. The word "gap" is used because this part of the spectrum remained unexplored for approximately forty years due to the lack of technology required to emit and detect this range of frequencies [11]. Nevertheless, optical and microwave technologies have made tremendous advances from the high and low frequency side in the last decades that allow us to study the properties and applications of this band of the spectrum [12, 13].

In this thesis four novel THz devices are presented. I present the design and experimental characterization of these four devices using 3D printing technology and terahertz time-domain spectroscopy. The fist device is a guided-mode filter, which depending on the physical dimensions, can be used to filter 200 GHz, 250 GHz or 300 GHz. Moreover, the filter could be linearly tuneable just by varying the angle between the incident beam and the waveguide. Furthermore, I present the design and experimental demonstration of three 3D printed devices to perform OR, AND and XOR logic operations at 130 GHz.

This thesis is organized in six chapters. Chapter 2 presents a brief perspective and outline of Terahertz radiation. I also dedicate this section to mention the techniques of emission and detection of Terahertz pulses emphasizing the use of photoconductive antennas. In addition, we include a section to describe the spectroscopic technique using THz pulses and some applications of THz radiation.

In chapter 3, an introduction to 3D printed technology is given as well

as some applications of this technology in the THz band. Finally, I mention some examples of 3D printing of THz passive components that scientists have made in recent years.

Chapter 4 presents the design, characterization and fabrication of a 3D printed guided-mode filter. I designed three devices to operate at 200 GHz, 250 GHz and 300 GHz. The devices were made of polystyrene, which is a material commonly used in 3D printing. The simulations and experimental measurements show that electromagnetic radiation propagating along the waveguide experiences a frequency selective process, resulting in a filter.

Chapter 5 includes the development of three different geometries to perform OR, AND and XOR logic operations. I also present in this chapter simulations computed in COMSOL Multiphysics in order to optimize the geometries. The logic gates were made of Bendlay, which is also a filament commonly used in the fabrication of 3D printed THz components. The logic gates as well as the filters were characterized and tested using a terahertz time-domain spectrometer in transmission configuration.

Chapter 6 presents the general conclusions of this work, where I highlight that 3D printing technology is an effective tool to produce novel components for control and manipulate THz radiation.

Chapter 2

The Terahertz Band

Terahertz (THz) radiation, also known as T-rays, are electromagnetic waves which lie between the microwave and infrared frequencies (300 GHz - 10 THz) [9, 14]. Figure 2.1 illustrates the THz band in the electromagnetic spectrum. Radiation at 1 THz has a period of 1 ps, a wavelength of 300 μm, a wavenumber of 33 cm^{-1}, a photon energy of 4.1 meV, and a temperature of 47.6 K [9]. THz radiation was not accessible until the mid 1980s due to the lack of efficient emitters and detectors for this band [10, 15]. On the microwaves side, electronic circuits are incapable of oscillating at such high frequencies and produce radiation in this band. On the other hand, quantum systems with low energy transitions are immersed in thermal noise, thus preventing them from being used as detectors unless they are cooled to cryogenic temperatures [16, 17]. Therefore, THz radiation has properties from both the electronic and photonic sides.

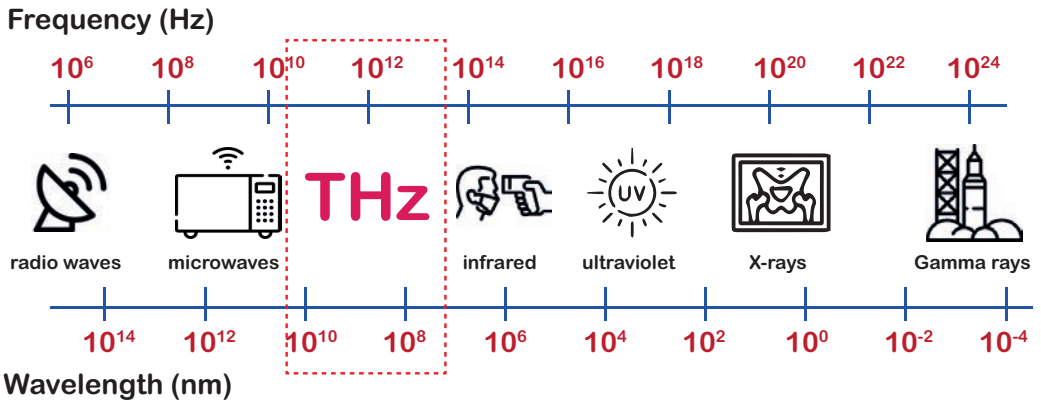

Figure 2.1: Electromagnetic spectrum. Bands of the spectrum from the low to high frequencies and long to short wavelengths. THz radiation is located between the microwave and infrared bands.

2.1 Emission and detection

Over the years, great efforts have been made to develop new techniques for emitting and detecting terahertz radiation [18, 19]. Generation and detection of THz radiation occur through nonlinear interaction of the driving optical pulse and a material with a fast response. For instance,Photoconductive (PC) antennas, some semiconductor surfaces, or quantum structures irradiated with femtosecond optical pulses [20, 21]. Most of the THz wave generation and detection systems consist of a pump and probe setup. These systems work by splitting the femtosecond laser beam into two beams: the pump and the probe beams. The pump beam is used to generate the THz pulse, while the probe beam is used to sample and detect the pulse profile [10, 22]. In this section an explanation of the process using PC antennas is given.

The PC antenna is one of the most commonly used emitters and detectors

for THz radiation [23, 20]. A PC antenna consists of two metallic electrodes placed on a semiconductor substrate. These electrodes are separated by a gap of a few microns and are connected to a bias voltage. In order to generate THz pulses, the optical pulse is absorbed on the antenna between the electrodes generating electron-hole pairs. These electron-hole pairs are accelerated towards the electrodes due to the potential difference, which produces a transient photo-current. This transient radiation has frequency components that fall in the THz band [24, 25].

The detection of THz pulses using PC antennas involves similar physical principles to those of their generation. The only major difference is that in the case of the detector, the two electrodes are connected to an amperimeter rather than a power supply. Again, electron-hole pairs are generated when the optical probe pulse reaches the gap on the antenna [26]. These free carriers are now accelerated by the THz pulse generating a photo-current which is proportional to the width of the THz beam. Since the THz pulse is almost 100 times longer than the optical pulse, the photo-induced carriers experience a steady electric field with amplitude equal to the value of the intersection with the THz pulse. Figure 2.2 illustrates the process of THz emission and detection using PC antennas.

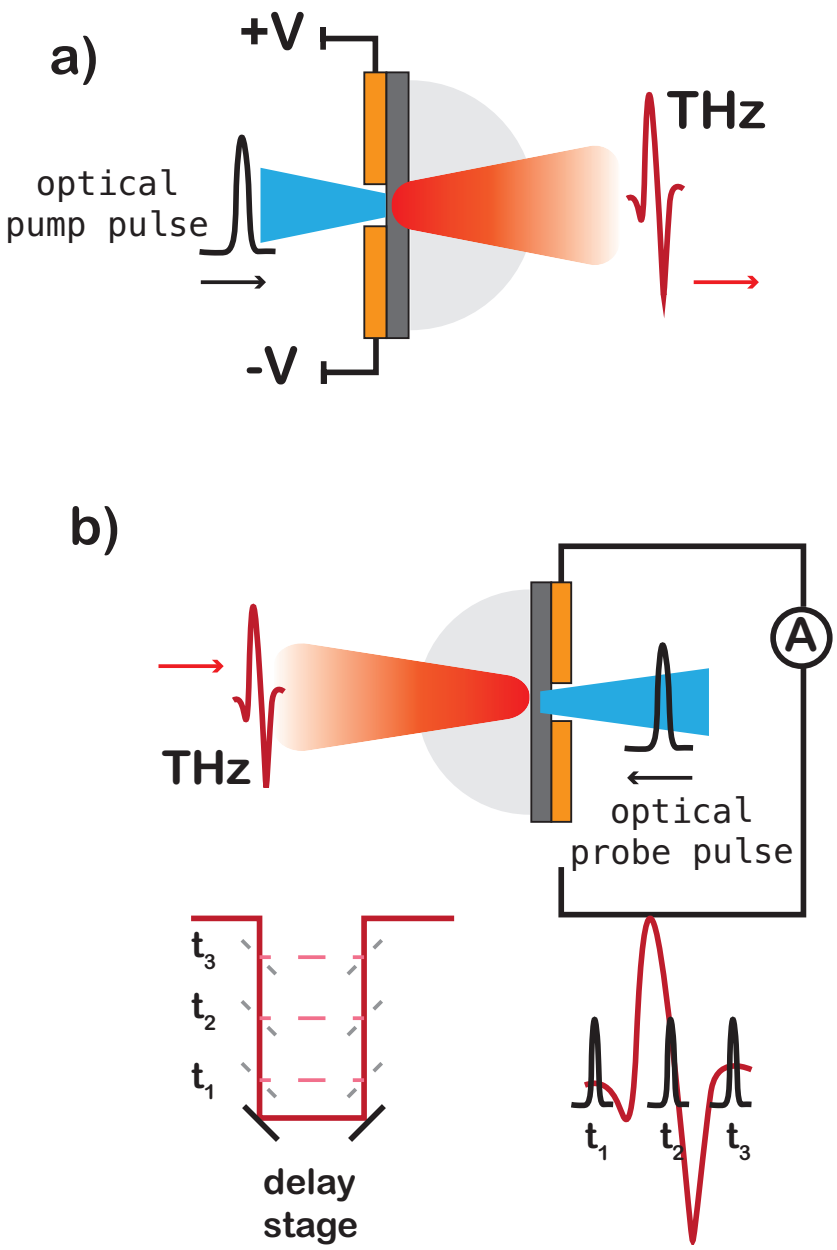

Figure 2.2: a) THz emission from PC antenna. b) Process of THz detection. The electric field measurement is determined by the arrival times t_1, t_2 and t_3 of the optical and THz pulse in time.

2.2 THz Time-Domain Spectroscopy

The continuous effort that scientists have made to develop techniques to generate and detect THz pulses has led us to the possibility of using them for spectroscopy [27, 28]. The spectroscopic technique using THz pulses is named Terahertz Time-Domain Spectroscopy (THz-TDS). One of the great advantages of THz-TDS as opposed to conventional Fourier transform spectroscopy is that it is able to measure not only the amplitude, but also the phase of the radiation [29]. This makes it possible to directly measure properties of the sample for instance its dispersion and refractive index [30]. The THz-TDS technique relies on the measurement of a short electromagnetic pulse that is transmitted, reflected or scattered by a sample. In this section we describe the experimental setup in transmission, since this is the setup used in this thesis.

A THz-TDS system consist of a femtosecond laser, a THz emitter and receiver, and a quasi-optical system that shapes the THz beam and directs it from the emitter, through the sample, to the receiver, and a delay stage that allows us to sample the signal.

The THz-TDS system used for this work has a laser that emit pulses with a duration of 10 to 100 fs, approximately. This laser generates pulses through the technique of mode locking. Figure 2.3 shows the THz-TDS system transmission setup.

THz-TDS makes it possible to directly measure the complex optical properties of the sample [31, 32]. In order to do this, a reference electric field $E_{ref}(t)$ is recorded without the sample. Subsequently, the sample is placed in between the emitter and detector and the transmitted electric field $E_{sam}(t)$

is recorded. In order to get the amplitude spectra of $E_{ref}(t)$ and $E_{sam}(t)$ in the frequency domain we compute the Fast Fourier Transform (FFT) of the reference and sample electric fields: $\tilde{E}_{ref}(\omega) = E_{ref}(\omega)e^{i\phi_{ref}(\omega)}$ and $\tilde{E}_{sam}(\omega) = E_{sam}(\omega)e^{i\phi_{sam}(\omega)}$.

The transfer function $\tilde{T}(\omega)$ of the sample in the frequency domain is given by equation 2.1

$$\tilde{T}(\omega) = \frac{\tilde{E}_{sam}(\omega)}{\tilde{E}_{ref}(\omega)} = \frac{E_{sam}(\omega)}{E_{ref}(\omega)} e^{i(\phi_{sam}(\omega) - \phi_{ref}(\omega))}. \tag{2.1}$$

The complex refractive index $\tilde{n}(\omega) = n(\omega) + i\kappa(\omega)$ can be directly calculated by equations 2.2 and 2.3

$$n(\omega) = 1 + \frac{c(\phi_{sample}(\omega) - \phi_{ref}(\omega))}{d\omega}, \tag{2.2}$$

$$\kappa(\omega) = -\frac{c}{2d\omega} ln \left[\frac{1}{t_{12}(\omega)t_{21}(\omega)} \frac{E_{sam}(\omega)}{E_{ref}(\omega)} \right]. \tag{2.3}$$

where $\phi_{sample}(\omega)$ and $\phi_{ref}(\omega)$ are the phase difference of the sample and reference signals, d is the thickness of the sample, $t_{12}(\omega)$ and $t_{21}(\omega)$ are the Fresnel transmission coefficients from air to sample and sample to air, respectively.

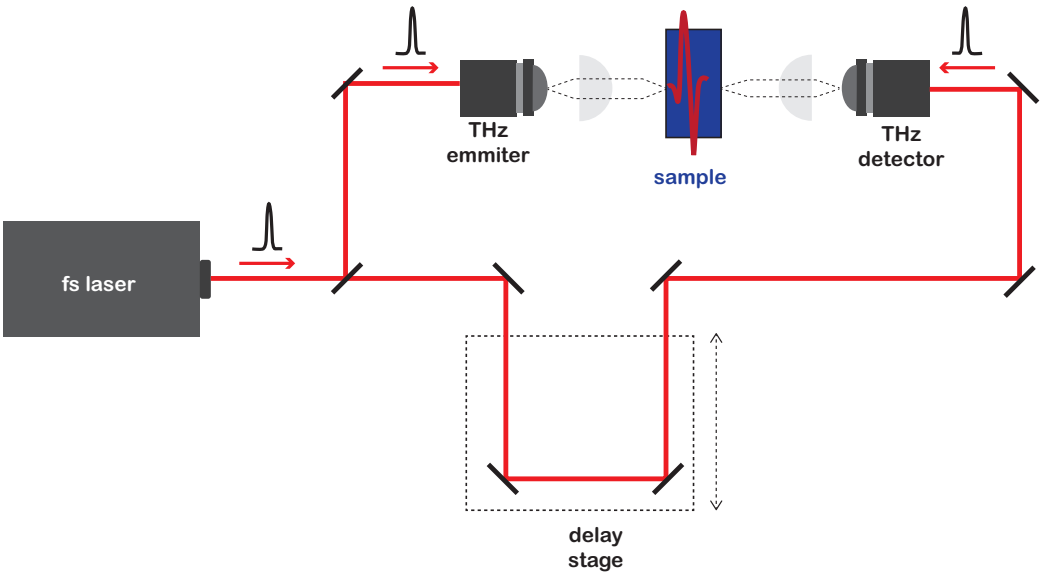

Figure 2.3: THz-TDS transmission setup. The femtosecond laser pulse is divided into an optical and pump pulse. The pump pulse is used to generate THz radiation, while the probe pulse is used for the detecting process. The lenses are used to direct the THz beam from the emitter to the receiver, passing through the sample.

2.3 Applications of THz radiation

Once sources and detectors of THz radiation were made available, scientists started to develop applications of this radiation. THz applications have been developed in different areas such as biomedical [33, 34], industrial [35, 36, 37], art conservation [38, 39], security [40, 41], among others. In this chapter we present some of these applications

- Biomedical: THz radiation does not present any health risks for scanning people [42, 43].This particular property has allowed scientists to use THz imaging for cancer detection [44, 45], skin hydration [46, 47] and biological tissue discrimination [48, 49].

- Security: Terahertz radiation can detect camouflaged weapons as many non-metallic materials are transparent to THz radiation. Furthermore, explosives and certain illegal drugs have characteristic THz spectra that can be used to identify these compounds [50, 51, 52].

- Industrial: THz-TDS allows characterization of samples with thicknesses of the order of the wavelength [53]. This characterization results useful in monitoring air voids in plastic structures [54] and for accurate thickness measurement of multi-layered automotive paints [55].

- Telecommunication: Nowadays digital data traffic continues increasing dramatically. In order to transmit growing amounts of data in accurate time, scientist are aiming to increase the available bandwidth. This leads to the development of new components to manipulate terahertz radiation. For instance, filters [56, 57], waveguides [58, 59], phase

modulators [60], polarizers [61], lenses [62], to name a few.

- Cultural heritage: It has been possible to analyze the internal structure of different types of paintings [63, 64, 65]. Terahertz has also been used to identify different artistic materials.

2.4 Conclusion

As we can see, due to the characteristics of this radiation, interesting applications have been developed. However, to continue developing and improving these and more applications it is indispensable the fabrication of optical components to manipulate THz radiation. Unfortunately, many materials that are transparent in the visible and infrared range turn out to be opaque at THz frequencies. Nevertheless, studies have shown that several polymers have favorable optical properties for the THz region [23]. This has given the possibility to manufacture devices and optical components for this region such as waveguides, lenses, polarizers, among others [66, 67, 68]. The aim of this thesis is to present the design, fabrication and characterization of four optical novel devices for terahertz frequencies. These devices corresponds to a guided-mode THz frequency filter and three optical logic gates that perform OR, AND and XOR logic operations.

Chapter 3

3D printing technology

3D printing, also known as additive manufacturing (AM), is a technology that has been used for many years for rapid prototyping [69, 70]. Compared with manufacturing technologies such as micromachining or spark erosion where objects are made in a subtracting manner, the principle of AM consist in building an object layer by layer. This has the advantage of consuming less energy and wasting less material [71, 72].

There exists a large range of AM techniques for rapid prototyping, including stereolithography (SLA) [73, 74], fusion deposition modeling (FDM) [75, 76], polymer jetting (PJ) [77, 78], electron beam melting (EBM) [79, 80], to mention just a few. Each technique varies in its procedure and has its advantages and disadvantages [81, 82]. In this thesis we used the FDM technique to fabricate passive devices that operate at THz frequencies. This technique has existed since 1980 and continues to be one of the most popular methods due to its high potential for fast prototyping [75, 83].

3.1 Fusion Deposition Modeling

The Fusion deposition modeling (FDM) is a rapid prototyping technique comercially developed by Stratasys in 1990 [84]. In order to print a three dimensional object we first create a digital model using a computer-aided design (CAD) interface. Next, the digital model is converted to an STL file. This file is a raw triangulation of the object and is used to create the calculation of the slices that make up the object to be printed. The next step is processing the STL file in order to transform it to a G-code. In this step the triangulation of the STL file are converted into a sequence of instructions executed by the printer. These instructions are basically a sequence of x, y and z coordinates plus a variable that controls the material injection. Inside the G-code, information about the printer settings is also present. For instance the nozzle temperature, bed temperature, positions of the steppers motors, the positions of the origin coordinates, speed of the printer, among others. Also, the trajectory of the printer is included in this code. This part of the code can be modified by the user using any mathematical software like Python, Octave, etc in order to choose a smart trajectory. By modifying the G-code directly it is possible to avoid the CAD design step and the STL file conversion.

For this work, we used both options. For the 3D printed terahertz filter we generate a txt file that that include the general parameters of the printer mentioned before, the trajectory followed by the nozzle and the final code to turn off all the components. For print the Terahertz Logic gates we used a CAD interface to design the geometries and then convert it to a STL file. The printing parameters such as the height and thickness, print speed,

printing temperature and fill density were controlled via a software to print 3D models.

Fusion deposition modeling technique consists in melting thermoplastic material, such as Acrylonitrile Butadiene Stirene (ABS) or Polylactic Acid (PLA), using a hot extruder nozzle. The nozzle hole diameter determines the resolution of the printer. In this work we used a nozzle with a hole diameter of $400\,\mu m$. The mechanism of FDM is made up of three axes: X, Y and Z. The X-Y plane is the base where the melted filament is deposited layer by layer and the Z-axis is used to control the height. The printing process starts with a first layer at $z = 0$, once this first layer has been deposited, a small amount of material is added in the z-direction in order to build a second layer and so on. Figure 3.1 illustrates the FDM technique and the elements that integrate the 3D printer.

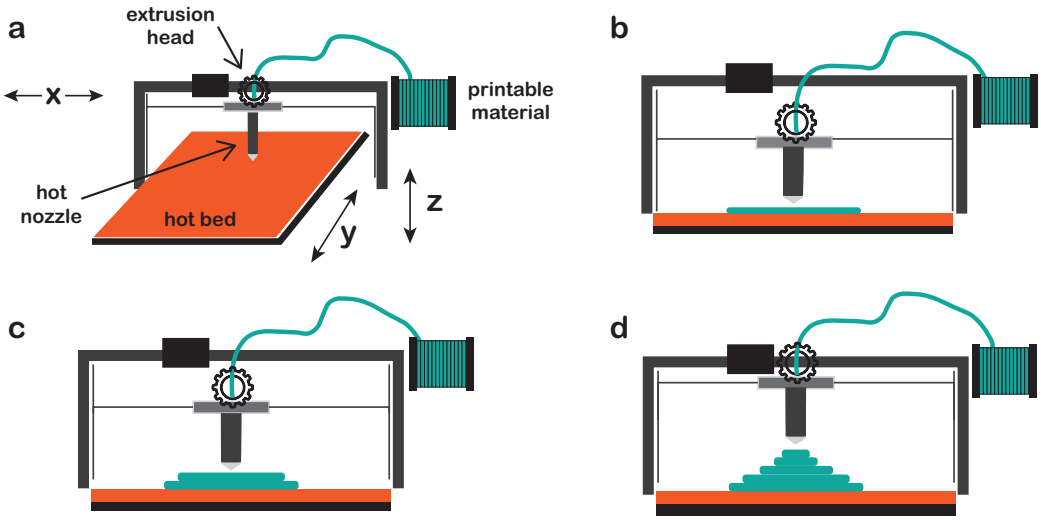

Figure 3.1: Diagram of a 3D printer. Figure (a) illustrates the main elements of the printer. Figures (b-d) show the process. The 3D printer builds the object layer by layer adding small amounts of printable material.

The printer used in this thesis was a Prusa i3 from Makermex, which is based on an open source model. The main elements of the printer are the printer bed and the extrusion head. The polymer filament is placed inside the extruder which uses a gear to pull the filament towards the nozzle. Near the nozzle, a heater and a thermistor are placed to control the temperature in order to melt the filament. Finally, the filament is extruded through the nozzle and deposited on the printing bed. For this work, a nozzle with a diameter of 0.4 mm was used. The movements along the X, Y, and Z directions are performed using stepper motors. The printer only moves in the Y direction, while the extrusion head moves in the X and Z directions.

As described above, the FDM technique is accessible and easy to implement. This has allowed scientists to use this technique to fabricate components that can be used in different areas. For instance, FDM 3D printing has been used for channel fabrication by bio-analytical and microfluidics researchers [85, 86]. Furthermore, in medical applications FDM has been used to fabricate implants that are used in oral and maxillofacial surgery and the development of artificial finger joints for orthopaedic applications [87, 88]. In this thesis we applied 3D technology in the field of optics to fabricate photonic devices. These devices are designed to operate at THz frequencies that make them able to be used in telecommunications.

3.2 THz passive devices

As mentioned in the previous chapter, terahertz radiation has been applied in different areas, such as telecommunications. The dramatical increase of digital data flow has led scientists to develop passive components that allow them to manipulate THz radiation in order to increase the bandwidths currently available [89, 90]. Over the last years, many efforts have been made in the development of photonic components for communications over the THz band. For instance, lenses [91, 92, 93], waveguides [94, 95], demultiplexers [96, 97] among others. On the other hand, 3D printing technology has attracted the attention of scientists and researchers because some polymers used in FDM turn out to be transparent to THz radiation [98, 99, 100]. Furthermore, the resolution of a simple and low-cost 3D printer ($\approx 400\mu m$) is enough to build THz components operating below $\approx 0.5\,THz$ due to large wavelength in the THz regime [101].

Lately, 3D printed dielectric waveguides and fibers have been reported for THz frequencies. For instance Weidenbach et al fabricated rectangular waveguides, splitters and couplers at 120 GHz using the FDM 3D printing technique [102]. In 2015 a hollow-core fiber with negative curvature was demonstrated by Cruz et al [103]. Furthermore, authors presented in [104] a 3D printed Bragg fiber for THz frequencies. All of these devices were fabricated with ABS and also by FDM technology. Moreover, various types of antennas have been fabricated using 3D printing technology [105, 106]. Unfortunately, most of the 3D printed antennas so far reported are above 0.1 THz due to the limit of state-of-the-art 3D printing technologies [101].

3.3 Conclusion

The development of printable polymers whose properties results favorable for the THz band open the possibility to fabricate optical devices, since 3D printing technique has the capability of creating complex geometrical structures. In the other hand, the consequence of the resolution of a FDM printer is that the fabricated devices operates only in the few hundred gigahertz region. This limitation can be overcome using other 3D printing techniques, but unfortunately increases manufacturing cost.

Chapter 4

Terahertz filters

In this section we report the design and fabrication of a 3D printed guided-mode filter for THz frequencies. We design three devices to operate at 200 GHz, 250 GHz and 300 GHz. These devices consist of a diffracting grating printed over a rectangular waveguide. The devices were made of polystyrene (PS), which is a material commonly used in 3D printed THz devices [98, 107]. We used a fiber-coupled time-domain spectrometer to characterize the devices. Simulations show, and the experimental measurements reinforce, that the coupling of electromagnetic radiation into the waveguide is highly frequency selective resulting in a frequency filter.

4.1 Design and modeling

When light travels from one medium to another, a portion of the light is reflected and a portion is transmitted into the second medium. As the transmitted light moves into a medium with different refractive index, it changes

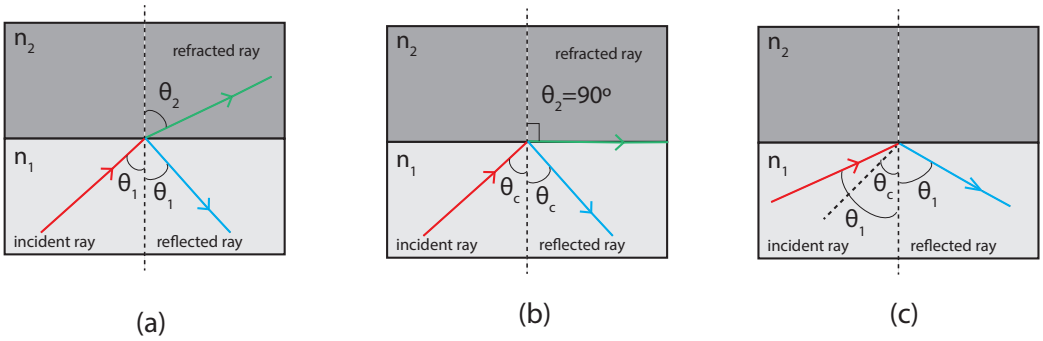

Figure 4.1: (a) When the angle of incidence is less than the critical angle, part of the light is refracted and part of the light is reflected. (b) The angle of incidence is equal to the critical angle, the angle of the refracted light reaches 90°. (c) When the angle of incidence is greater than the critical angle, light is totally reflected back into the medium.

its direction of travel. This means it is refracted. Snell's law describes the relationship between the angle of incidence and the angle of refraction.

When light is refracted from a medium of higher refractive index to a medium of lower refractive index, the angle of refraction is greater than the angle of incidence. As the angle of incidence approaches a certain limit, called the critical angle, the angle of refraction approaches 90°, at which the refracted ray becomes parallel to the surface. As the angle of incidence increases beyond the critical angle, the conditions of refraction can no longer be satisfied; so there is no refracted ray, and the partial reflection becomes total reflection.

Figure 4.1 explains schematically how total internal reflection takes place in an interface between two media. An incident ray (red) goes into an interface and part of the light is reflected (blue) and refracted (green). When the

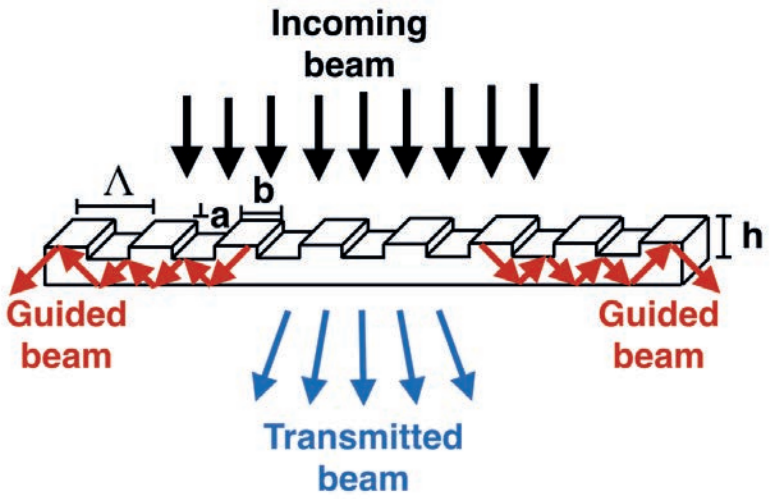

Figure 4.2: Simplified diagram of the proposed device. The exit angle of some of the diffracted modes at a particular frequency satisfies the total internal reflection condition inside the waveguide.

angle of incidence θ_1 is greater than the critical angle θ_c, the light is totally reflected back to the medium.

In the other hand, when a wave is incident on a grating, it diffracts into a finite number of modes called spatial harmonics or diffraction orders. The angles of the diffracted modes θ_m are described by the grating equation 4.1

$$n_t sin(\theta_m) = n_{inc} sin\theta_{inc} - \frac{m\lambda_0}{\Lambda}, \tag{4.1}$$

where $n_t = 1.56$ is the refractive index of the grating, $\theta(m)$ is the diffractive angle of the m-th diffracted mode, $n_{inc} = 1$ is the refractive index of the external medium, θ_{inc} is the angle of incidence of the electromagnetic beam, λ is the vacuum wavelength and Λ is the period of the grating [108].

Figure 4.2 shows the principle of operation of the filter, where w and h are the width and height of the rectangular waveguide; a, b and Λ are the height, width and the period of the grating. An electromagnetic beam is coupled laterally through the waveguide. If the exit angle of the diffracted mode is higher or equal to the total internal reflection angle inside the waveguide, then the electromagnetic radiation will be confined and will propagate in the waveguide. The effective refractive index of the waveguide is given by equation 4.2

$$n_{eff} = n_t sin(\theta) = n_t sin(\theta(m)). \tag{4.2}$$

Given that $n_{inc} \leq n_{eff} \leq n_t$ and combining equation 4.1 and equation 4.2, the condition to be satisfied for any particular wavelength to be guided inside the waveguide is

$$n_{inc} \leq |n_{inc} sin(\theta_{inc}) - m\frac{\lambda}{\Lambda}| \leq n_t. \tag{4.3}$$

In order to analyze the functionality of the filters we set the period of the grating to $\Lambda = 0.8\,mm$ to filter 300 GHz. This parameter was selected using equation 4.3. The height and width of the grating $a = 0.2\,mm$, $b = 0.4\,mm$ were chosen taken into account the nozzle diameter of the 3D printer. We also set in the simulation the width and height of the waveguide to $w = 0.8\,mm$ and $h = 1\,mm$. These dimensions were chosen to have single-mode operation and the propagation length of the waveguide was 5 cm.

We computed three simulations using the filter previously described at 250 GHz, 300 GHz and 350 GHz in order to analyzed the functionality of the filter around 300 GHz. A plane wave was propagated by our simulation

through the top of the grating. Figure 4.3 a)-c) shows the simulations results for 250 GHz, 300 GHz and 350 GHz for a plane wave parallel to the grating. According to the simulations the electric field amplitude at the right-hand side relative to the incoming amplitude are 0.2, 0.8 and 0.1 for 250 GHz, 300 GHz and 350 GHz respectively. These results show that the coupling of the 250 GHz and 350 GHz beams into the waveguide are relatively low, while the coupling at 300 GHz is comparatively strong. This is consistent with the theoretical analysis done before where the condition of equation 4.3 is satisfied at 300 GHz for the first diffraction order $m = 1$.

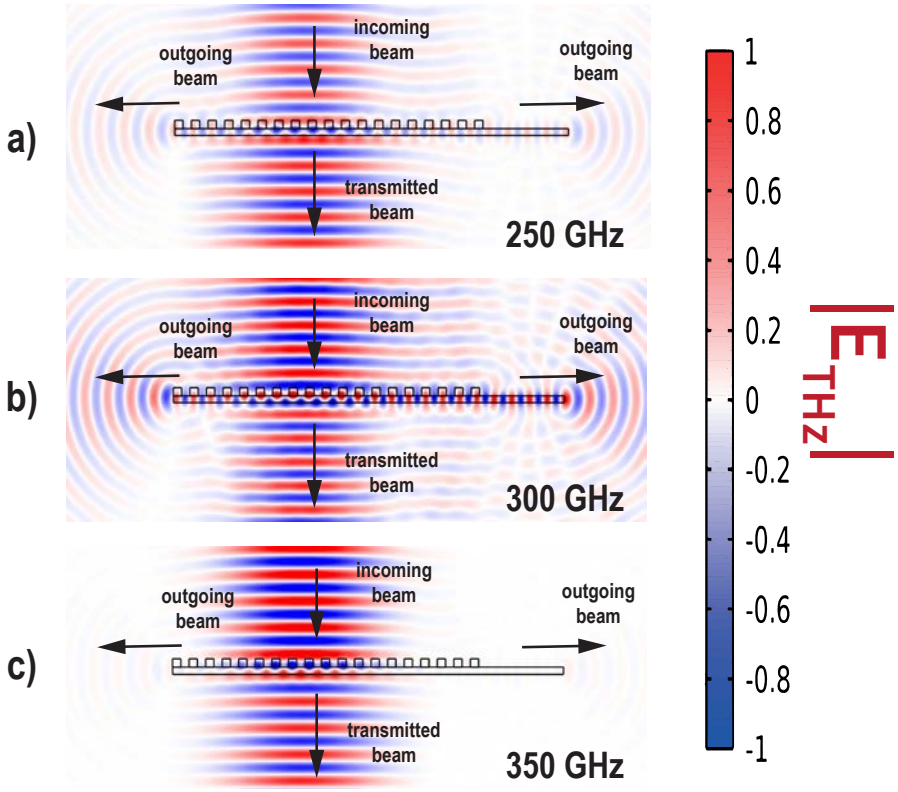

Figure 4.3: Simulation results for a device to act as a filter at 300 GHz when illuminated at a) 250 GHz, b)300 GHz and c)350 GHz.

4.2 Fabrication and characterization

We used the Fusion Deposition Modeling (FDM) technique, which is widely described in chapter 3, and a Prusa i3 3D printer to fabricate the filters. These filters were made of polystyrene (PS), which has a refractive index of 1.56 between 0.2 THz and 3 THz and an absorption coefficient of $0.4\,cm^{-1}$ at 500 GHz [98].

We decided to print three different devices to operate at 200 GHz, 250 GHz and 300 GHz. We set the height and width of the rectangular waveguide to $h = 1\,mm$ and $w = 0.8\,mm$; the height and width of the grating to $a = 0.2\,mm$ and $b = 0.4\,mm$, and the propagation length of the waveguide was $5\,cm$ for each device. The only parameter that we modified in each of the filters was the period of the grating. For 200 GHz we set the period to $\Lambda_{200} = 1.2\,mm$; for 250 GHz we set the period to $\Lambda_{250} = 1\,mm$ and for 300 GHz we set the period of the grating to $\Lambda_{300} = 0.8\,mm$. All these parameters were optimized by the simulation software and equation 4.3. Figure 4.4 a) shows one of the printed filters. Is worth to mention that in order to filter higher frequencies the period of the grating decrease. In this particular work, the spatial resolution of the 3D printer ($400\,\mu m$) does not allowed to print a filter for frequencies above 300 GHz. Therefore, we choose 200 GHz, 250 GHz and 300 GHz to carry out the characterization of the filters.

We used a fiber-coupled time-domain spectrometer in transmission configuration, to characterize the devices. We recorded the THz pulses after propagation through the filters. Figure 4.4 b) shows a simplified diagram of the experimental setup. We used 25.5 mm focal length High Density Polyethylene (HDPE) lenses in order to focus the THz beam parallel to the grating.

Also, we placed an aperture in front of the receiver in order to ensure that we were only detecting the radiation that came from the waveguide. The filter was placed away from the focal position of the transmitter lens to guarantee a wider interaction region between the THz beam and the grating.

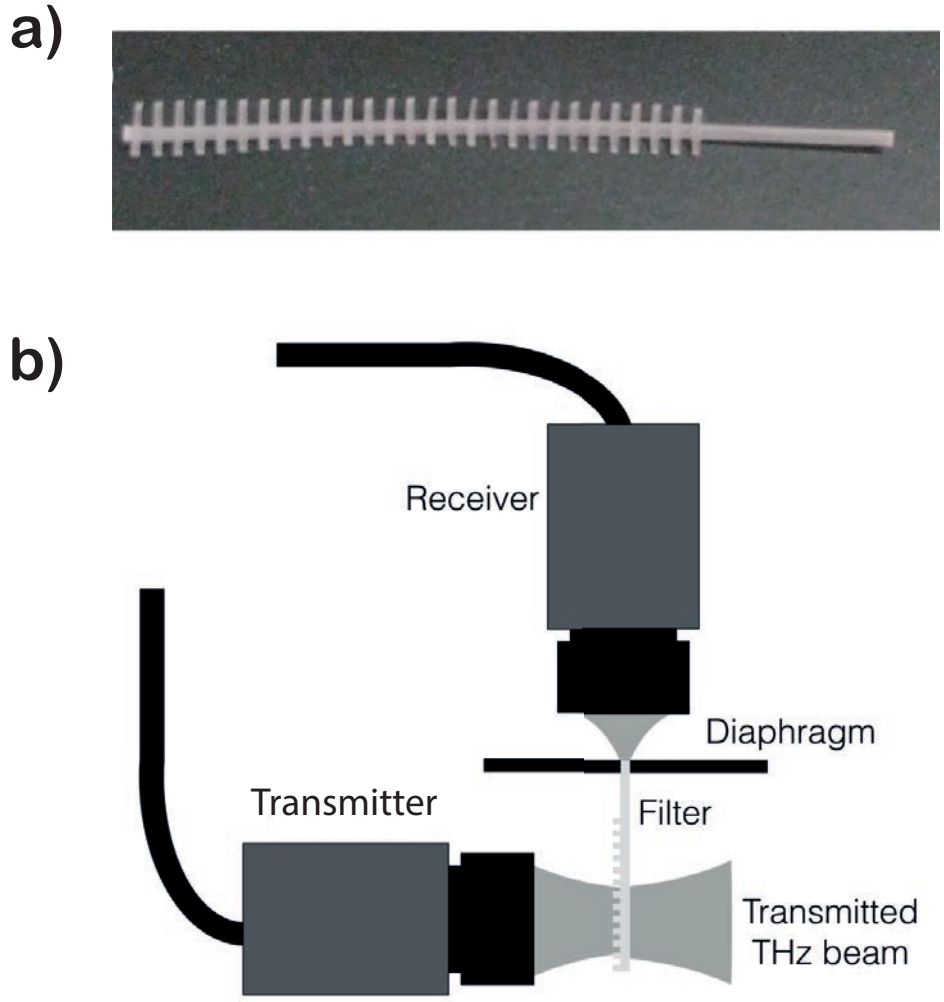

Figure 4.4: a) 3D printed filter for 200 GHz. b) Experimental setup used to characterize the 3D printed filters.

4.3 Results

From the previous measurements we obtained the THz pulses in the time domain for each filter and we computed their amplitude spectra in the frequency domain by Fourier Transform. Figure 4.5a and 4.5b shows the THz pulses and its amplitude spectra corresponding to each waveform. The dashed lines in Figure 4.5b correspond to the experimental measurements while the solid lines are the simulated results. We can see in the graph many similarities between experimental and numerical results. Using this data we estimated the Q-factor of each filter to be 2.6 (6.45), 4.5 (6.4) and 4.5 (8.3) experimentally (theoretically) for 200 GHz, 250 GHz and 300 GHz, respectively. The difference that occurs between the experimental and theoretical values of the Q factor is due to the widening of the experimental spectra. Moreover, as mentioned, the incoming beam was placed away from the focal position. This led to a coupling efficiency of 21%, 25% and 28% for these frequencies. The filter whose experimental and numerical curves show the greatest difference is the 300GHz device. This is caused by imperfections in the fabricated devices inherent to the 3D printing technique.

Another interesting property of these filters is that the position of the coupling peak depends linearly on the angle between the incoming beam and the waveguide axis. This dependence is given by equation 4.4. From this equation it is clear that the position of the peak varies linearly depending on the angle between the incoming beam and the waveguide axis of the filter.

$$\frac{\Delta\lambda}{\Delta\theta_{inc}} = \frac{n_{inc}\Lambda}{m}. \tag{4.4}$$

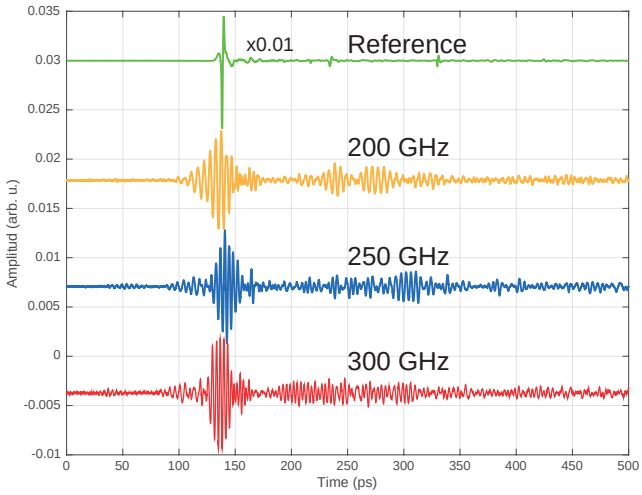

(a) THz pulses corresponding to the experimental measurements.

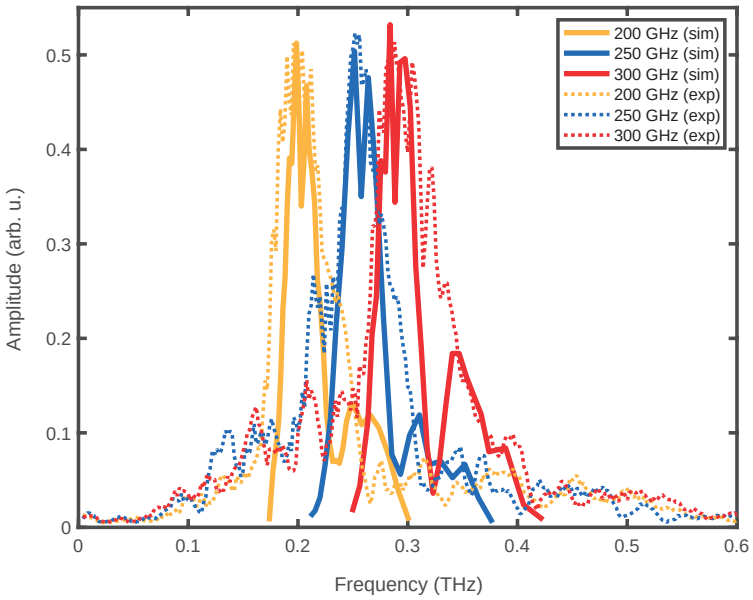

(b) Amplitude spectra corresponding to the THz pulses.

Figure 4.5: Experimental results of the filters at 200 GHz, 250 GHz and 300 GHz.

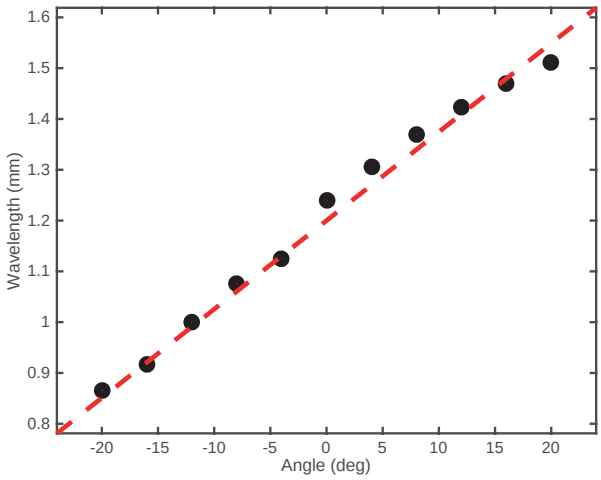

Figure 4.6: Central wavelength as a function of the incidence angle. The dots are the experimental values and the dashed line is the expected position of the central peak predicted by equation 4.4.

To prove this property we used the same experimental setup shown in figure 4.4 and the 250 GHZ filter. In this experiment we hold the transmitter on a rotational stage in order to vary the incidence angle from $-20°$ to $20°$ in steps of $4°$. Figure 4.6 shows the peak wavelengths as circles which indicate a linear behaviour consistent with the dashed line, which is the predicted position of the resonant wavelength as a function of the incidence angle given by equation 4.4.

4.4 Conclusions

In this chapter we presented the design and experimental demonstration to fabricate a plastic filter for terahertz frequencies fabricated by 3D printing technology. The filters are made up of a grating printed over a rectangular single-mode waveguide. Depending on the period of the grating the devices behave as a filter at 200 GHz, 250 GHz and 300 GHz. These devices can be used for the construction of THz frequency tunable filters for telecommunication applications, among others. Finally, this work provides further evidence that 3D printing technology is a powerful tool for the design and fabrication of novel THz devices which can be used in different applications.

Chapter 5

Terahertz logic gates

In this section we present the design of three 3D printed logic gates that perform the logic operations OR, AND, XOR and NOT at 130 GHz. Recently, optical logic gates have been demonstrated based on various techniques and materials. For instance, electromagnetic simulations of optical logic gates in metal slot waveguides have been proposed in [109, 110, 111] for the near infrared spectrum. Moreover, logic gates based on two-dimensional (2D) photonic crystals [112, 113, 114], graphene nanoribbons [115, 116], and semiconductor optical amplifiers [117, 118] have been proposed and numerically investigated by finite difference time-domain (FDTD) simulations. Additionally, logic operations at THz frequencies with a reconfigurable geometry based on micro/nano electromechanical systems have been proposed in [119]. In this work, we propose simple, low cost solutions to perform logic operations at THz frequencies using three-dimensional (3D) printing technology.

The principle of operation of these photonic logic gates consists of two input waveguides that couple to a series of particular geometries making the

radiation interfere in such a way that the output signal follows the desired logic rule. The cross-section of the input and output waveguides were designed in order to have single mode operation. In order to optimize the geometries of the designs for the desired logical operations, we used COMSOL Multiphysics. Once the geometries were optimized we used a Prusa i3 3D printer to fabricate three different devices to perform the OR, AND and XOR operations. The devices were made out of Bendlay, which is a translucent material commonly used in fused deposition modeling 3D printing [101, 100]. The experimental characterization was carried out with a THz-TDS spectrometer in transmission configuration. The simulations and experimental measurements show a good agreement between numerical and experimental data.

5.1 Design and modeling

The structures of the devices consist of two input dielectric waveguides that couple radiation that interfere properly to obtain the desired logical operation. Each logic gate has four input combinations: "on/on", "on/off", "off/on" and "off/off", where "on/off" indicates radiation "coupled/not-coupled" in the corresponding input waveguides. In the OR gate an "on" output results if one or both inputs of the gate are "on". If neither input is "on", an "off" output results. In the AND gate, an "on" output results only if all the inputs are "on". The XOR gate implements an exclusive OR; that is an "on" output results if one and only one of the inputs of the gate is "on". In all cases the output signal is the radiation that results from the interference

of these input combinations. Figure 5.1 shows the 3D printed geometry of these logic gates.

The geometries of the OR and XOR gate are similar. Both of them have an input rectangular waveguide of 27 mm, a second input with a slightly curved shape and an output rectangular waveguide of a length of 5 mm. The difference between them is that compared to its first input waveguide, the second input of the OR gate has a path length difference of $\lambda/3$ in order to have a similar amplitude at the output when both input waveguides are on and when just one input waveguide is on. In the case of the XOR logic gate we add to a path length of $\lambda/2$ in order to have destructive interference when both input waveguides are on. We were aware to maintain the radius of the curvatures of the waveguides larger than 2λ with the purpose of preventing leakage.

The AND geometry consist of two input rectangular waveguides of a length of 20 mm, a rectangle of $8.5 \times 13.2\,mm$ where the two inputs interfere and an output waveguide length of 10 mm. The dimensions of this rectangle were chosen in order to obtain a 1×2 multimode interference splitter, but in this case operating the other way around. The input and output cross-section of the three devices are $1.5\,mm \times 1.5\,mm$ and were chosen using a parametric-sweep in the simulation software with the purpose of having single mode operation.

In order to optimize these geometries, we used COMSOL Multiphysics to compute the electric field distribution of the OR, AND and XOR logic gates at 130 GHz. COMSOL uses the Finite Element Method to approximate the solution of the propagation of the electromagnetic wave in the frequency

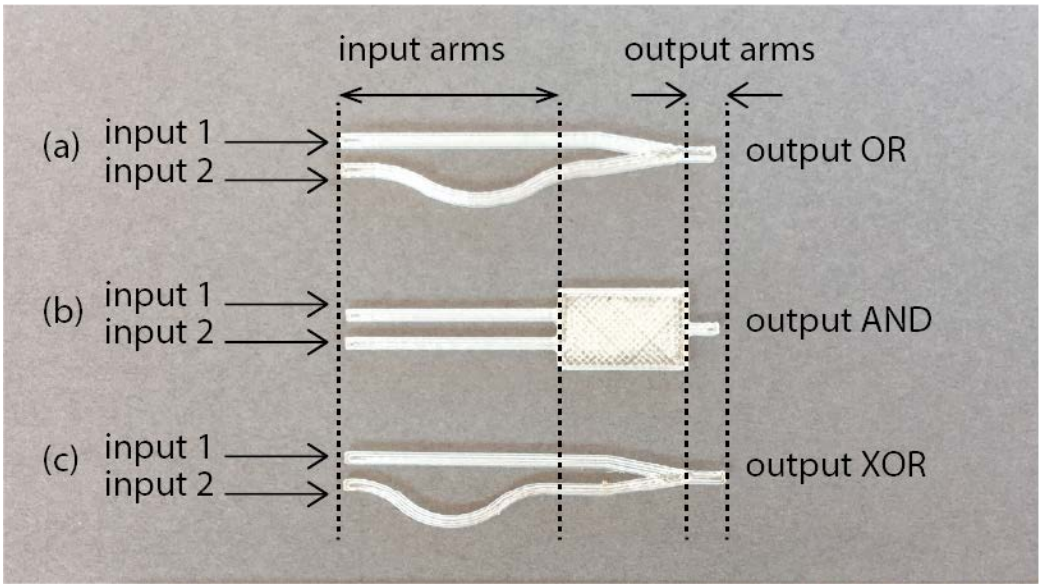

Figure 5.1: Geometries of the (a)OR, (b) AND and (c) XOR printed photonic logic gates. The operational principle consist of two input waveguides that interfere to obtain the desired output operation. The width of the waveguide is 1.5 mm.

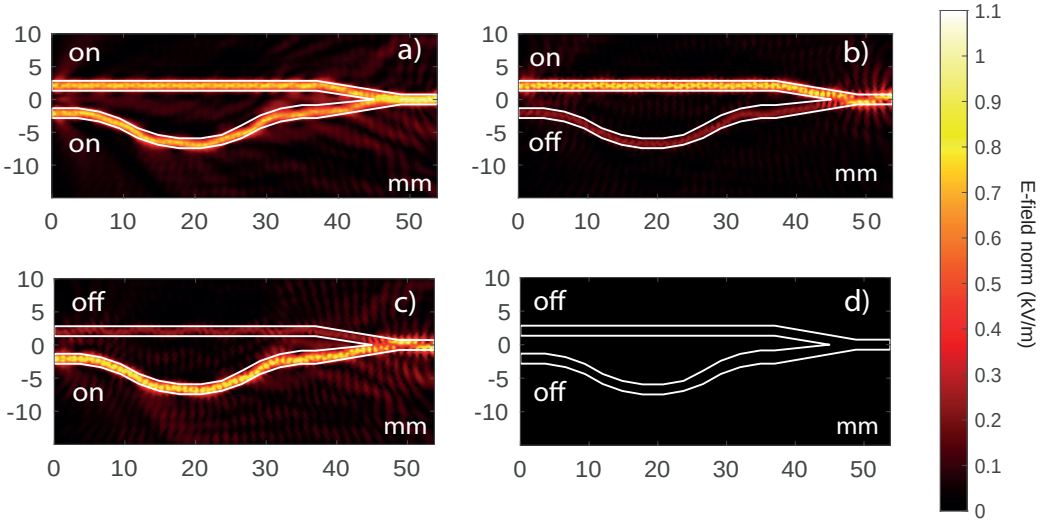

Figure 5.2: Electric field distribution for OR logic gate simulation at 130 GHz. Panels a)-d) represent the four input combinations "on/on", "on/off", "off/on" and "off/off", respectively.

domain. For this study we performed a 2-dimensional analysis since we have almost axi-symmetric geometries and we set scattering boundary condition for all the boundaries outside the geometries.

In addition, 2D simulations are computationally less demanding and therefore faster to solve than a 3D model. We defined two input ports at the beginning of the geometries in order to perform the four input combinations and one output port in order to evaluate the output electric field at the end of the devices. These ports were defined as TE10 waveguides modes where the vector direction of the E-field is out-of-plane.

The simulation results for the OR logic gate are shown in Figure 5.2. The color map of panel a) represents the input combinations "on/on" where the field is mostly distributed in the two input arms. Next, the two input waveg-

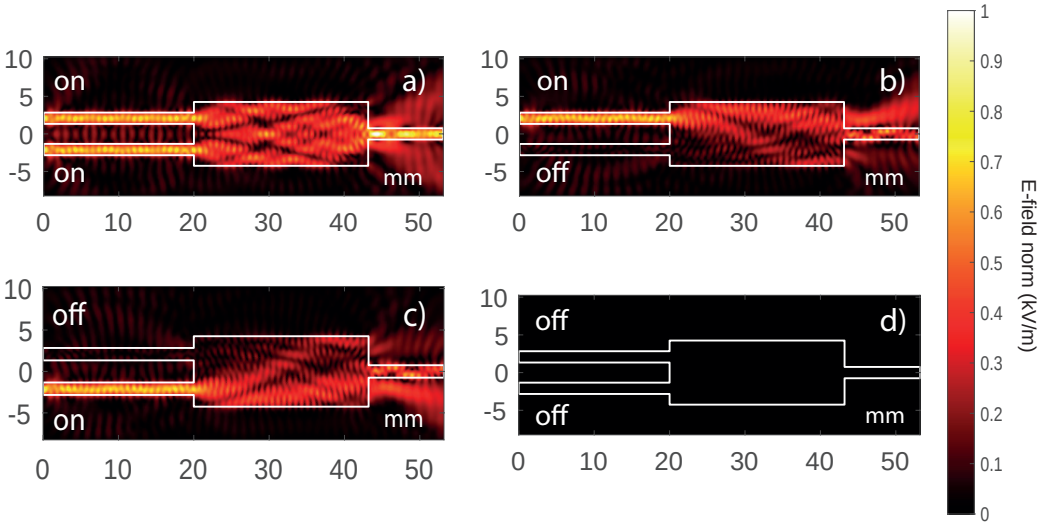

Figure 5.3: Electric field distribution for AND logic gate simulation at 130 GHz. Panels a)-d) represent the four input combinations "on/on", "on/off", "off/on" and "off/off", respectively.

uides are joined in a "y" shape where the radiation interferes constructively to get an output state "on". The second and third input combinations are shown in panels b) and c), where we only coupled radiation in one input arm. The simulation shows that the electric field again propagates almost uniformly inside the input waveguide until the end of the device, resulting also in an "on" output state. Finally, when both inputs are "off" we get a 0-amplitude at the end of the OR gate as shown panel d).

Figure 5.3 shows the simulations results for the logic operation AND at 130 GHz. Panel a) shows the input operation "on/on", where the interference pattern is symmetric. Both input waveguides are in phase and interfere constructively. Therefore, the radiation couples in the output port producing an output state "on". Panels b) and c) of Figure 5.3 shown the input combina-

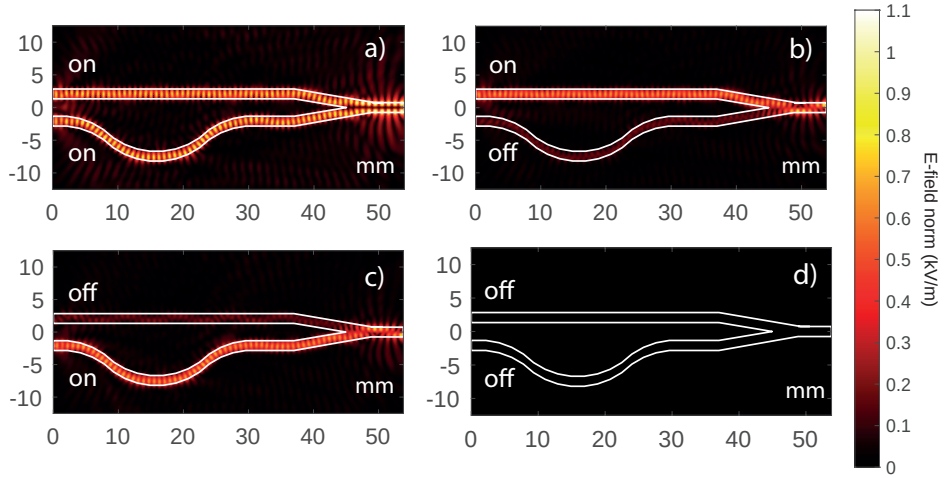

Figure 5.4: Electric field distribution for XOR logic gate simulation at 130 GHz. Panels a)-d) represent the four input combinations "on/on", "on/off", "off/on" and "off/off", respectively.

tions "on/off" and "off/on" respectively. In these operations, when radiation is coupled just in one input waveguide, the input waveguide do not interfere with any other signal and propagates within the rectangle. Although radiation is still coupled at the output waveguide, it is $< 40\%$ compared to the incoming radiation. This small portion of coupled radiation is enough to be interpreted as an output state "off". Finally, panel d) of Figure 5.3 shows the case when both input waveguides are "off" and as expected, the output at the end of the waveguide is "off".

Finally, Figure 5.4 shows the simulation results for the XOR logic gate also at 130 GHz. Compared with the OR logic gate, the XOR operation has an output "off" when radiation is coupled into the two input waveguides, as shown in panel a). In this case we built the second input arm in such

a way that the two input waves have a de-phase of $\lambda/2$. This implies that we obtain destructive interference at the output waveguide, and therefore an output state "off". Panels b) and c) are similar to Figure 5.2 where radiation is mostly distributed into the input waveguides until the end of the device giving an output state "on". Panel d) of OR, AND and XOR logic gates represent the operation with input combination "off"/"off", which means no radiation is coupling in any of the input waveguides resulting in a zero or "off" output state.

5.2 Fabrication and characterization

Once the devices were optimized, we used a Prusa i3 3D printer to fabricate the OR, AND and XOR logic gates. The devices were made of Bendlay, which has a refractive index of 1.54 and an absorption coefficient of $0.4\,cm^{-1}$ at THz frequencies [100]. The 3D geometries were designed in FreeCAD according to the parameters from the previous simulations and exported to a STL format. Subsequently, we used CURA software to "slice" the 3D models which produced a G-code file. Finally, this file was read by the printer, and it was possible to begin the printing process. For the printing process we set a layer height of 0.1 mm, print speed of 25 mm/ s and the nozzle and bed temperatures to 235° C and 60° C, respectively.

In order to characterize the 3D printed logic gates, we used a THz-TDS spectrometer in transmission configuration. As described before, the logic operations consist of two inputs and one output. This means that in theory we need two sources. To overcome this difficulty, since we only have one source,

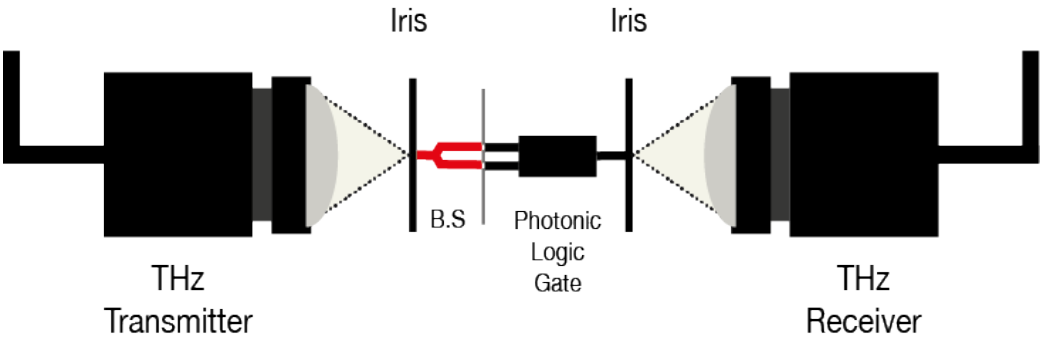

Figure 5.5: Experimental setup used to characterize the 3D printed logic gates.

we designed a 50/50 3D printer beam splitter to couple the THz beam into the two input waveguides. Between the beam splitter and the logic gate we left a gap of $\sim \lambda$ where we placed a metallic sheet in order to block Input 1, Input 2 or both so that we could perform the four input combinations of the logic OR, AND and XOR operations. The experimental setup is illustrated in Figure 5.5. The metallic sheet was placed in a x-y translational platform in order to control the input combinations. To perform the "on/on" operation, the metallic sheet moved completely to one side allowing both input waveguides to be coupled to the beam splitter. In order to perform "on/off" and "off/on" operations, the translational platform moved the metallic sheet to one side or the other blocking just one input waveguide. Finally, the input combination "off/off" is achieved by blocking both inputs with the metallic sheet, therefore, no THz radiation propagates through the devices.

To test the devices, we obtained the amplitude spectra of the four input combinations for each 3D printed THz logic gate. Since the spectrometer provides electric amplitude measurements in arbitrary units, for clarity and

simplicity, the value of 1 will correspond to the amplitude of the OR gate with the input combination "on/on" and we will call these normalized amplitudes. For this work, we considered the amplitudes equal or greater than 0.5 as an output "on" and below 0.5 as an output "off". Figure 5.6 shows the output amplitudes of the OR, AND and XOR logic gates. Each color represents an input combination "on/on", "on/off", "off/on" and "off/off". Panels (a-c) represent the numerical amplitudes from simulations, and panels (d-f) are the experimental amplitudes measured with the spectrometer. We placed a horizontal dashed line as a guide regarding the amplitude threshold that divides the values above as an output "on" and the values below this line as output "off". The vertical continuous blue line indicates the position of the frequency at 130 GHz, which is the design operation frequency.

5.3 Results

Comparing numerical and experimental data, we can observe that these curves are considerably similar despite in the form frequency shifts. The differences between the numerical and experimental curves occurs for three main reasons. First, the simulations assume a flat input spectrum, while in the experimental measurements, the spectrometer has a characteristic spectral response. Secondly, the coupling efficiency into the waveguides is wavelength dependent. And thirdly, the imperfections in the printed devices that are inherent to the 3D printing technique. Figure 5.6 (d) shows the experimental amplitudes of the OR gate for the input combinations "on/on", "on/off", and "off/on", where the output amplitude is above 0.8 resulting in

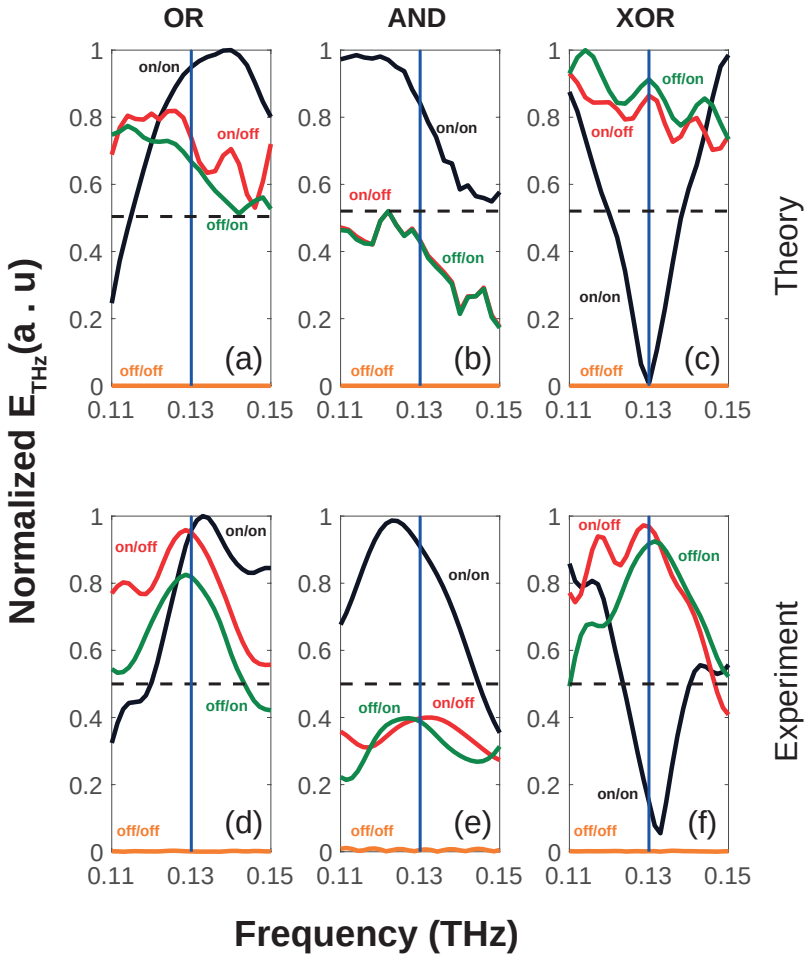

Figure 5.6: Normalized amplitudes (a-c) simulated and (d-f) measured at the output port for all input combinations "on/off" for the OR, AND and XOR logic gates; dashed lines indicate the threshold that defines outputs values "on" and "off at 130 GHz.

an "on" output as we expected. The input combination "off/on" is around 0.1 below the input combination "on/off". This loss can be attributed to the curvature that we introduced in the second input waveguide. Nevertheless, the output amplitude is above the defined threshold.

Panel (e) of the same figure shows the experimental characterization of the AND logic gate. In this case an output value "on" occurs only with the input combination "on/on". The input combinations "on/off" (in red) and "off/on" (in green) show an amplitude ~ 0.4, which, according to the previous definition, is assumed to be an "off" output, as well as the input combination "off/off".

Finally, panel (f) shows the experimental output amplitudes for the XOR logic gate. It is clear that the input combination "on/on" at 130 GHz produces an output value "off" compared to the input operations "on/off" and "off/on" whose amplitudes are above 0.9. Once again, the output amplitude of the "off/on" input combination is slightly lower compared to the output amplitude of "on/off" due to the curvature in the second input waveguide.

We can observe that the amplitude of the signals varies at different frequencies. In most of the cases, the amplitude decays as we move away from 130 GHz. This is due to the fact that we designed the rectangular waveguides of these geometries to operate at this particular frequency. However, they can be rescalable to operate at other frequencies. Lastly, is worth to mention that the XOR geometry can also operate as a NOT gate. Unlike AND, OR and XOR, the NOT gate has only one input. This means that it compute just two operations: when the input is "on" the output is "off" and vice versa. Then if we take one of the input waveguides of the XOR as the

input waveguide of the NOT and we let the second input waveguide always "on" we obtain the outputs of the NOT logic operation.

5.4 Conclusions

In this chapter we introduced three different waveguide geometries to perform OR, AND and XOR logic operations at 130GHz. The geometries were optimized, fabricated by 3D printing technology and tested using THz-TDS. All three devices successfully performed the logic operations. The OR and XOR gates show a notorious contrast between the "on" and "off" output states. Nonetheless, the AND gate does not present such a great contrast between the "on/off" and "off/on" input states, the relative output amplitude is below the threshold previously defined. Moreover, it is worth mentioning that the XOR logic gate can also perform the NOT operation when one of the input waveguides is kept in the on state.

Some advantages of these geometries over other logic gates for terahertz frequency is that these geometries are easily rescalable for operation at higher or lower frequencies. Also, since they are made of plastic, they are easy to mass produce by mould fabrication. Furthermore, the cost of fabrication is extremely low compared to semiconductor based devices. Finally, it is possible to build larger photonic circuits using these three devices, since they can be integrated using more complex geometries without requiring additional fabrication technologies.

Chapter 6

Conclusions

Our world is rapidly transforming into a society that depends on information. For this reason, optical signal processing plays and will continue playing an important role in the future. In this thesis I presented four novel devices for terahertz frequencies fabricated by 3D printing technology. The first is a frequency filter. I demonstrated that, depending on the physical dimensions of the device, it can be used to filter different frequencies in the terahertz range. We also successfully fabricated and characterized three devices to filter 200 GHz, 250 GHz and 300 GHz. Moreover, tuneability of a single device can be also achieved just by varying the angle between the incoming beam and the device. This opens the possibilities for fabricating terahertz tuneable filters for telecommunications, among other applications.

Furthermore, in order to send information and to transmit it and process from a medium to another, it must be digitized, that is, represented by sequences of zeros and ones. This is why photonic logic gates are necessary. Moreover, these gates should offer high processing speeds that allow secure

communications with higher bandwidths and using fewer energy resources, which will be reflected in manufacturing costs. Trying to overcome this problem, we presented in this thesis three different 3D printed devices that perform the OR, AND and XOR logic operations. The design of these devices is based on rectangular waveguides that produce the correct interference behaviour for the radiation from the input ports of the devices in order to obtain the desired output. The simplicity of the geometries allows for scaling the dimensions of the devices to operate at different frequencies. Moreover, the same geometry design of the XOR logic gate can also be used as a NOT gate by leaving one input waveguide always in the "on" state and performing the input combinations "on" and "off" with the second input waveguide. Logic gates are essential components for performing all-optical functions. These basic designs integrated together, may lead to more complex digital operations. Furthermore, we have been working on integrating these logic gates to create an adder circuit. So far we have designed a half adder circuit using the AND and XOR logic gate. However, we are still working on the optimization of the dimensions to have a greater contrast in the outputs and low dispersion along the circuit.

In this thesis I demonstrated that I could efficiently use fusion deposition 3D printing technique to fabricate optical components that operate at THz frequencies that can be used in telecommunications. By using this technology I can acquire great advantages such as reducing the cost and manufacturing time of these devices. In addition, the fact that these devices can operate at THz frequency helps to increase the bandwidth currently available, which is necessary due to the enormous amount of data that we use these days.

Bibliography

[1] C. Roychoudhuri, A. Kracklauer, and K. Creath, *The Nature of Light What is a Photon?* CRC Press, 2008, ISBN: 9780367387105.

[2] J. J. THOMSON, "The nature of light," *Nature*, vol. 137, Feb. 1936. DOI: 10.1038/137232a0. [Online]. Available: https://doi.org/10.1038/137232a0.

[3] E. Hecht, *Optics*, 4th. Addison-Wesley, 1998.

[4] R. Longhurst, *Geometrical and Physical Optics*, 3rd. Longman, 1973, out of print.

[5] R. Guenther, *Modern Optics*. Wiley, 1990.

[6] K. M.V. and T. Furtak, *Optics*, 2nd ed. Wiley, 1986.

[7] B. E. A. Saleh and M. C. Teich, *Fundamentals of Photonics*, 2nd ed. Wiley, 2007.

[8] A. Babin and A. Figotin, *Neoclassical Theory of Electromagnetic Interactions*, 1st ed. Springer, 2016.

[9] Y.-S. Lee, *Principles of Terahertz Science and Technology*, 1st. Springer Publishing Company, Incorporated, 2008, ISBN: 038709539X.

[10] X.-C. Zhang and J. Xu, *Introduction to THz Wave Photonics*. Springer US, 2010.

[11] T. Elsaesser, K. Reimann, and M. Woerner, *Concepts and Applications of Nonlinear Terahertz Spectroscopy*, ser. 2053-2571. Morgan & Claypool Publishers, 2019, ISBN: 978-1-64327-216-0. DOI: 10.1088/2053-2571/aae931. [Online]. Available: http://dx.doi.org/10.1088/2053-2571/aae931.

[12] R. A. Lewis, *Terahertz Physics*. Cambridge University Press, 2013. DOI: 10.1017/CBO9781139088190.

[13] K. Sakay, *Terahertz Optoelectroncs*, 1st ed. Springer-Verlag Berlin Heidelberg, 2005. DOI: 10.1007/b80319.

[14] M. Hangyo, T. Nagashima, and S. Nashima, "Spectroscopy by pulsed terahertz radiation," *Measurement Science and Technology*, vol. 13, no. 11, pp. 1727–1738, Oct. 2002. DOI: 10.1088/0957-0233/13/11/309. [Online]. Available: https://doi.org/10.1088/0957-0233/13/11/309.

[15] J. Neu and C. A. Schmuttenmaer, "Tutorial: An introduction to terahertz time domain spectroscopy (thz-tds)," *Journal of Applied Physics*, vol. 124, no. 23, p. 231 101, 2018. DOI: 10.1063/1.5047659. eprint: https://doi.org/10.1063/1.5047659. [Online]. Available: https://doi.org/10.1063/1.5047659.

[16] S. L. Dexheimer, *Terahertz Spectroscopy: Principles and Applications*. CRC Press Taylor and Francis Group, 2008.

[17] J. Madéo, A. Margiolakis, Z.-Y. Zhao, P. J. Hale, M. K. L. Man, Q.-Z. Zhao, W. Peng, W.-Z. Shi, and K. M. Dani, "Ultrafast properties of femtosecond-laser-ablated gaas and its application to terahertz optoelectronics," *Opt. Lett.*, vol. 40, no. 14, pp. 3388–3391, Jul. 2015. DOI: 10.1364/OL.40.003388. [Online]. Available: http://ol.osa.org/abstract.cfm?URI=ol-40-14-3388.

[18] T. Otsuji, T. Watanabe, S. A. Boubanga Tombet, A. Satou, W. M. Knap, V. V. Popov, M. Ryzhii, and V. Ryzhii, "Emission and detection of terahertz radiation using two-dimensional electrons in iii–v semiconductors and graphene," *IEEE Transactions on Terahertz Science and Technology*, vol. 3, no. 1, pp. 63–71, 2013. DOI: 10.1109/TTHZ.2012.2235911.

[19] T. Otsuji, T. Watanabe, S. A. B. Tombet, A. Satou, V. Ryzhii, V. V. Popov, and W. Knap, "Emission and detection of terahertz radiation using two-dimensional plasmons in semiconductor nanoheterostructures for nondestructive evaluations," *Optical Engineering*, vol. 53, no. 3, pp. 1–14, 2013. DOI: 10.1117/1.OE.53.3.031206. [Online]. Available: https://doi.org/10.1117/1.OE.53.3.031206.

[20] K. Sakai and M. Tani, "Introduction to terahertz pulses," in *Terahertz Optoelectronics*, K. Sakai, Ed. Berlin, Heidelberg: Springer Berlin Heidelberg, 2005, pp. 1–30, ISBN: 978-3-540-31488-2. DOI: 10.1007/10828028_1. [Online]. Available: https://doi.org/10.1007/10828028_1.

[21] A. S. Weling and D. H. Auston, "Novel sources and detectors for coherent tunable narrow-band terahertz radiation in free space," *J. Opt. Soc. Am. B*, vol. 13, no. 12, pp. 2783–2792, Dec. 1996. DOI: 10.1364/JOSAB.13.002783. [Online]. Available: http://josab.osa.org/abstract.cfm?URI=josab-13-12-2783.

[22] H. Němec, F. Kadlec, and P. Kužel, "Methodology of an optical pump-terahertz probe experiment: An analytical frequency-domain approach," *The Journal of Chemical Physics*, vol. 117, no. 18, pp. 8454–8466, 2002. DOI: 10.1063/1.1512648. eprint: https://doi.org/10.1063/1.1512648. [Online]. Available: https://doi.org/10.1063/1.1512648.

[23] E. Castro-Camus and M. Alfaro, "Photoconductive devices for terahertz pulsed spectroscopy: A review [invited]," *Photon. Res.*, vol. 4, no. 3, A36–A42, Jun. 2016. DOI: 10.1364/PRJ.4.000A36. [Online]. Available: http://www.osapublishing.org/prj/abstract.cfm?URI=prj-4-3-A36.

[24] T. Masahiko, "Photoconductive emission and detection of terahertz pulsed radiation using semiconductors and semiconductor devices," *Journal of Infrared, Millimeter, and Terahertz Waves*, vol. 33, Apr. 2012. DOI: 10.1007/s10762-012-9882-1. [Online]. Available: https://doi.org/10.1007/s10762-012-9882-1.

[25] N. M. Burford and M. O. El-Shenawee, "Review of terahertz photoconductive antenna technology," *Optical Engineering*, vol. 56, no. 1,

pp. 1–20, 2017. DOI: 10.1117/1.OE.56.1.010901. [Online]. Available: https://doi.org/10.1117/1.OE.56.1.010901.

[26] Y. Huang, N. Khiabani, Y. Shen, and D. Li, "Terahertz photoconductive antenna efficiency," in *2011 International Workshop on Antenna Technology (iWAT)*, 2011, pp. 152–156. DOI: 10.1109/IWAT.2011.5752384.

[27] M. C. Nuss and J. Orenstein, "Terahertz time-domain spectroscopy," in *Millimeter and Submillimeter Wave Spectroscopy of Solids*, G. Grüner, Ed. Berlin, Heidelberg: Springer Berlin Heidelberg, 1998, pp. 7–50, ISBN: 978-3-540-68710-8. DOI: 10.1007/BFb0103419. [Online]. Available: https://doi.org/10.1007/BFb0103419.

[28] M. Naftaly and R. E. Miles, "Terahertz time-domain spectroscopy for material characterization," *Proceedings of the IEEE*, vol. 95, no. 8, pp. 1658–1665, 2007. DOI: 10.1109/JPROC.2007.898835.

[29] M. Tani, M. Herrmann, and K. Sakai, "Generation and detection of terahertz pulsed radiation with photoconductive antennas and its application to imaging," *Measurement Science and Technology*, vol. 13, no. 11, pp. 1739–1745, Oct. 2002. DOI: 10.1088/0957-0233/13/11/310. [Online]. Available: https://doi.org/10.1088%2F0957-0233%2F13%2F11%2F310.

[30] L. Duvillaret, F. Garet, and J. .-.-. Coutaz, "A reliable method for extraction of material parameters in terahertz time-domain spectroscopy," *IEEE Journal of Selected Topics in Quantum Electronics*, vol. 2, no. 3, pp. 739–746, 1996. DOI: 10.1109/2944.571775.

[31] L. Duvillaret, F. Garet, and J.-L. Coutaz, "Highly precise determination of optical constants and sample thickness in terahertz time-domain spectroscopy," *Appl. Opt.*, vol. 38, no. 2, pp. 409–415, Jan. 1999. DOI: 10.1364/AO.38.000409. [Online]. Available: http://ao.osa.org/abstract.cfm?URI=ao-38-2-409.

[32] P. Y. Han, M. Tani, M. Usami, S. Kono, R. Kersting, and X.-C. Zhang, "A direct comparison between terahertz time-domain spectroscopy and far-infrared fourier transform spectroscopy," *Journal of Applied Physics*, vol. 89, no. 4, pp. 2357–2359, 2001. DOI: 10.1063/1.1343522. eprint: https://doi.org/10.1063/1.1343522. [Online]. Available: https://doi.org/10.1063/1.1343522.

[33] J. F. Federici, B. Schulkin, F. Huang, D. Gary, R. Barat, F. Oliveira, and D. Zimdars, "THz imaging and sensing for security applications—explosives, weapons and drugs," *Semiconductor Science and Technology*, vol. 20, no. 7, S266–S280, Jun. 2005. DOI: 10.1088/0268-1242/20/7/018. [Online]. Available: https://doi.org/10.1088%2F0268-1242%2F20%2F7%2F018.

[34] R. O. Alfonsina and G. G. Piero, "Terahertz radiation effects and biological applications," *Journal of Infrared, Millimeter, and Terahertz Waves*, vol. 30, Dec. 2009. DOI: 10.1007/s10762-009-9561-z. [Online]. Available: https://doi.org/10.1007/s10762-009-9561-z.

[35] S. Wietzke, C. Jansen, C. Jördens, N. Krumbholz, N. Vieweg, M. Scheller, M. K. Shakfa, D. Romeike, T. Hochrein, M. Mikulics, and M. Koch, "Industrial applications of THz systems," in *International*

Symposium on Photoelectronic Detection and Imaging 2009: Terahertz and High Energy Radiation Detection Technologies and Applications, X.-C. Zhang, J. M. Ryan, C.-l. Zhang, and C.-x. Tang, Eds., International Society for Optics and Photonics, vol. 7385, SPIE, 2009, pp. 56–68. DOI: 10.1117/12.840991. [Online]. Available: https://doi.org/10.1117/12.840991.

[36] M. Naftaly, N. Vieweg, and A. Deninger, "Industrial applications of terahertz sensing: State of play," *Sensors*, vol. 19, no. 19, 2019, ISSN: 1424-8220. DOI: 10.3390/s19194203. [Online]. Available: https://www.mdpi.com/1424-8220/19/19/4203.

[37] B. Robert, "Sensing with terahertz radiation: A review of recent progress," *Sensor Review*, vol. 38, Jan. 2018. DOI: 10.1108/SR-10-2017-0221. [Online]. Available: https://doi.org/10.1108/SR-10-2017-0221.

[38] K. Fukunaga, N. Sekine, I. Hosako, N. Oda, H. Yoneyama, and T. Sudou, "Real-time terahertz imaging for art conservation science," *Journal of the European Optical Society - Rapid publications*, vol. 3, no. 0, 2008, ISSN: 1990-2573. [Online]. Available: http://www.jeos.org/index.php/jeos_rp/article/view/08027.

[39] K. Fukunaga and M. Picollo, "Erahertz spectroscopy applied to the analysis of artists' materials," *Applied Physics A*, vol. 100, 2010, ISSN: 1432-0630. [Online]. Available: https://doi.org/10.1007/s00339-010-5643-y.

[40] M. C. Kemp, P. F. Taday, B. E. Cole, J. A. Cluff, A. J. Fitzgerald, and W. R. Tribe, "Security applications of terahertz technology,"

in *Terahertz for Military and Security Applications*, R. J. Hwu and D. L. Woolard, Eds., International Society for Optics and Photonics, vol. 5070, SPIE, 2003, pp. 44–52. DOI: 10.1117/12.500491. [Online]. Available: https://doi.org/10.1117/12.500491.

[41] H. Liu, H. Zhong, N. Karpowicz, Y. Chen, and X. Zhang, "Terahertz spectroscopy and imaging for defense and security applications," *Proceedings of the IEEE*, vol. 95, no. 8, pp. 1514–1527, 2007. DOI: 10.1109/JPROC.2007.898903.

[42] O. P. Cherkasova, D. S. Serdyukov, A. S. Ratushnyak, E. F. Nemova, E. N. Kozlov, Y. V. Shidlovskii, K. I. Zaytsev, and V. V. Tuchin, "Effects of terahertz radiation on living cells: A review," *Optics and Spectroscopy*, vol. 128, 2020. DOI: 10.1134/S0030400X20060041.

[43] E. Pickwell and V. P. Wallace, "Biomedical applications of terahertz technology," *Journal of Physics D: Applied Physics*, vol. 39, no. 17, R301–R310, Aug. 2006. DOI: 10.1088/0022-3727/39/17/r01. [Online]. Available: https://doi.org/10.1088/0022-3727/39/17/r01.

[44] L. Yu, L. Hao, T. Meiqiong, H. Jiaoqi, L. Wei, D. Jinying, C. Xueping, F. Weiling, and Z. Yang, "The medical application of terahertz technology in non-invasive detection of cells and tissues: Opportunities and challenges," *RSC Adv.*, vol. 9, pp. 9354–9363, 17 2019. DOI: 10.1039/C8RA10605C. [Online]. Available: http://dx.doi.org/10.1039/C8RA10605C.

[45] B. B. Hu and M. C. Nuss, "Imaging with terahertz waves," *Opt. Lett.*, vol. 20, no. 16, pp. 1716–1718, Jun. 1995. DOI: 10.1364/OL.20.

001716. [Online]. Available: http://ol.osa.org/abstract.cfm?URI=ol-20-16-1716.

[46] Q. Sun, Y. He, K. Liu, S. Fan, E. P. J. Parrott, and E. Pickwell-MacPherson, "Recent advances in terahertz technology for biomedical applications," *Quantitative imaging in medicine and surgery*, vol. 7, 2017, ISSN: 2223-4292. [Online]. Available: https://pubmed.ncbi.nlm.nih.gov/28812001.

[47] Z. D. Taylor, R. S. Singh, D. B. Bennett, P. Tewari, C. P. Kealey, N. Bajwa, M. O. Culjat, A. Stojadinovic, H. Lee, J. .-.-P. Hubschman, E. R. Brown, and W. S. Grundfest, "Thz medical imaging: In vivo hydration sensing," *IEEE Transactions on Terahertz Science and Technology*, vol. 1, no. 1, pp. 201–219, 2011. DOI: 10.1109/TTHZ.2011.2159551.

[48] E. Pickwell and V. P. Wallace, "Biomedical applications of terahertz technology," *Journal of Physics D: Applied Physics*, vol. 39, no. 17, R301–R310, Aug. 2006. DOI: 10.1088/0022-3727/39/17/r01. [Online]. Available: https://doi.org/10.1088%2F0022-3727%2F39%2F17%2Fr01.

[49] D. B. Bennett, W. Li, Z. D. Taylor, W. S. Grundfest, and E. R. Brown, "Stratified media model for terahertz reflectometry of the skin," *IEEE Sensors Journal*, vol. 11, no. 5, pp. 1253–1262, 2011. DOI: 10.1109/JSEN.2010.2088387.

[50] J. F. Federici, B. Schulkin, F. Huang, D. Gary, R. Barat, F. Oliveira, and D. Zimdars, "THz imaging and sensing for security applications—explosives,

weapons and drugs," *Semiconductor Science and Technology*, vol. 20, no. 7, S266–S280, Jun. 2005. DOI: 10.1088/0268-1242/20/7/018. [Online]. Available: https://doi.org/10.1088%2F0268-1242%2F20%2F7%2F018.

[51] D. A. Zimdars, "Fiber-pigtailed terahertz time domain spectroscopy instrumentation for package inspection and security imaging," in *Terahertz for Military and Security Applications*, R. J. Hwu and D. L. Woolard, Eds., International Society for Optics and Photonics, vol. 5070, SPIE, 2003, pp. 108–116. DOI: 10.1117/12.519632. [Online]. Available: https://doi.org/10.1117/12.519632.

[52] M. Kowalski, "Hidden object detection and recognition in passive terahertz and mid-wavelength infrared," *Journal of Infrared, Millimeter, and Terahertz Waves*, vol. 40, 2019. DOI: 10.1007/s10762-019-00628-7.

[53] M. Perenzoni and D. Paul, *Physics and Applications of Terahertz Radiation*, 1st. Springer Netherlands, 2014, ISBN: 978-94-017-7915-9.

[54] N. Pałka, A. Rybak, T. Jakubowski, M. Florkowski, M. Kowalski, P. Zagrajek, M. Życzkowski, W. Ciurapiński, L. Jodłowski, and M. Walczakowski, "Monitoring of air voids at plastic-metal interfaces by terahertz radiation," *Infrared Physics & Technology*, vol. 104, p. 103 119, 2020, ISSN: 1350-4495. DOI: https://doi.org/10.1016/j.infrared.2019.103119. [Online]. Available: http://www.sciencedirect.com/science/article/pii/S135044951930619X.

[55] S. Krimi, J. Klier, J. Jonuscheit, G. von Freymann, R. Urbansky, and R. Beigang, "Highly accurate thickness measurement of multi-layered automotive paints using terahertz technology," *Applied Physics Letters*, vol. 109, no. 2, p. 021 105, 2016. DOI: 10.1063/1.4955407. eprint: https://doi.org/10.1063/1.4955407. [Online]. Available: https://doi.org/10.1063/1.4955407.

[56] A. Ferraro, A. A. Tanga, D. C. Zografopoulos, G. C. Messina, M. Ortolani, and R. Beccherelli, "Guided mode resonance flat-top bandpass filter for terahertz telecom applications," *Opt. Lett.*, vol. 44, no. 17, pp. 4239–4242, Sep. 2019. DOI: 10.1364/OL.44.004239. [Online]. Available: http://ol.osa.org/abstract.cfm?URI=ol-44-17-4239.

[57] J. Li, Y. Li, and L. Zhang, "Terahertz bandpass filter based on frequency selective surface," *IEEE Photonics Technology Letters*, vol. 30, no. 3, pp. 238–241, 2018. DOI: 10.1109/LPT.2017.2782774.

[58] M. A. K. Othman, M. C. Hoffmann, M. E. Kozina, X. J. Wang, R. K. Li, and E. A. Nanni, "Parallel-plate waveguides for terahertz-driven mev electron bunch compression," *Opt. Express*, vol. 27, no. 17, pp. 23 791–23 800, Aug. 2019. DOI: 10.1364/OE.27.023791. [Online]. Available: http://www.opticsexpress.org/abstract.cfm?URI=oe-27-17-23791.

[59] S. Li and T. E. Murphy, "Graphene-based waveguide-integrated terahertz modulator," *ACS Photonics*, vol. 4, Feb. 2017. DOI: doi:10.

1021/acsphotonics.6b00751. [Online]. Available: https://doi.org/10.1021/acsphotonics.6b00751.

[60] I.-C. Benea-Chelmus, T. Zhu, F. F. Settembrini, C. Bonzon, E. Mavrona, D. L. Elder, W. Heni, J. Leuthold, L. R. Dalton, and F. A. PhotonicsJérôme, "Three-dimensional phase modulator at telecom wavelength acting as a terahertz detector with an electro-optic bandwidth of 1.25 terahertz," *ACS Photonics*, vol. 5, Apr. 2018. DOI: doi:10.1021/acsphotonics.7b01407. [Online]. Available: https://doi.org/10.1021/acsphotonics.7b01407.

[61] G. Wu, Y. Zeng, K. F. Chan, S. Qu, and C. H. Chan, "3-d printed circularly polarized modified fresnel lens operating at terahertz frequencies," *IEEE Transactions on Antennas and Propagation*, vol. 67, no. 7, pp. 4429–4437, 2019. DOI: 10.1109/TAP.2019.2908110.

[62] H. Yi, S. Qu, K. Ng, C. H. Chan, and X. Bai, "3-d printed millimeter-wave and terahertz lenses with fixed and frequency scanned beam," *IEEE Transactions on Antennas and Propagation*, vol. 64, no. 2, pp. 442–449, 2016. DOI: 10.1109/TAP.2015.2505703.

[63] K. Fukunaga and I. Hosako, "Innovative non-invasive analysis techniques for cultural heritage using terahertz technology," *Comptes Rendus Physique*, vol. 11, no. 7, pp. 519–526, 2010, Terahertz electronic and optoelectronic components and systems, ISSN: 1631-0705. DOI: https://doi.org/10.1016/j.crhy.2010.05.004. [Online]. Available: http://www.sciencedirect.com/science/article/pii/S1631070510000460.

[64] J. B. Jackson, J. Bowen, G. Walker, J. Labaune, G. Mourou, M. Menu, and K. Fukunaga, "A survey of terahertz applications in cultural heritage conservation science," *IEEE Transactions on Terahertz Science and Technology*, vol. 1, no. 1, pp. 220–231, 2011. DOI: 10.1109/TTHZ.2011.2159538.

[65] K. Krügener, M. Schwerdtfeger, S. F. Busch, A. Soltani, E. Castro-Camus, M. Koch, and W. Viöl, "Terahertz meets sculptural and architectural art: Evaluation and conservation of stone objects with t-ray technology," *Scientific Reports*, vol. 5, no. 2045-2322, 2015. DOI: 10.1038/srep14842.

[66] A. I. Hernandez-Serrano, M. Weidenbach, S. F. Busch, M. Koch, and E. Castro-Camus, "Fabrication of gradient-refractive-index lenses for terahertz applications by three-dimensional printing," *J. Opt. Soc. Am. B*, vol. 33, no. 5, pp. 928–931, May 2016. DOI: 10.1364/JOSAB.33.000928. [Online]. Available: http://josab.osa.org/abstract.cfm?URI=josab-33-5-928.

[67] A. I. Hernandez-Serrano, Q. Sun, E. G. Bishop, E. R. Griffiths, C. P. Purssell, S. J. Leigh, J. Lloyd-Hughes, and E. Pickwell-MacPherson, "Design and fabrication of 3-d printed conductive polymer structures for thz polarization control," *Opt. Express*, vol. 27, no. 8, pp. 11 635–11 641, Apr. 2019. DOI: 10.1364/OE.27.011635. [Online]. Available: http://www.opticsexpress.org/abstract.cfm?URI=oe-27-8-11635.

[68] R. Guo, E.-M. Stuebling, F. Beltran-Mejia, D. Ulm, T. Kleine-Ostmann, F. Ehrig, and M. Koch, "3d printed terahertz rectangular waveguides of polystyrene and topas: A comparison," *Journal of Infrared, Millimeter, and Terahertz Waves*, vol. 40, Jan. 2019. DOI: 10.1007/s10762-018-0552-9. [Online]. Available: https://doi.org/10.1007/s10762-018-0552-9.

[69] T. D. Ngo, A. Kashani, G. Imbalzano, K. T. Nguyen, and D. Hui, "Additive manufacturing (3d printing): A review of materials, methods, applications and challenges," *Composites Part B: Engineering*, vol. 143, pp. 172–196, 2018, ISSN: 1359-8368. DOI: https://doi.org/10.1016/j.compositesb.2018.02.012. [Online]. Available: http://www.sciencedirect.com/science/article/pii/S1359836817342944.

[70] M. P. Browne, E. Redondo, and M. Pumera, "3d printing for electrochemical energy applications," *Chemical Reviews*, vol. 120, no. 5, pp. 2783–2810, 2020, PMID: 32049499. DOI: 10.1021/acs.chemrev.9b00783. eprint: https://doi.org/10.1021/acs.chemrev.9b00783. [Online]. Available: https://doi.org/10.1021/acs.chemrev.9b00783.

[71] B. Zhang, Y. Guo, H. Zirath, and Y. P. Zhang, "Investigation on 3-d-printing technologies for millimeter- wave and terahertz applications," *Proceedings of the IEEE*, vol. 105, no. 4, pp. 723–736, 2017. DOI: 10.1109/JPROC.2016.2639520.

[72] L. F. Arenas, F. C. Walsh, and C. P. de León, "3d-printing of redox flow batteries for energy storage: A rapid prototype laboratory cell," *ECS Journal of Solid State Science and Technology*, vol. 4, no. 4, P3080–P3085, 2015. DOI: 10.1149/2.0141504jss. [Online]. Available: https://doi.org/10.1149/2.0141504jss.

[73] R. He, W. Liu, Z. Wu, D. An, M. Huang, H. Wu, Q. Jiang, X. Ji, S. Wu, and Z. Xie, "Fabrication of complex-shaped zirconia ceramic parts via a dlp- stereolithography-based 3d printing method," *Ceramics International*, vol. 44, no. 3, pp. 3412–3416, 2018, ISSN: 0272-8842. DOI: https://doi.org/10.1016/j.ceramint.2017.11.135. [Online]. Available: http://www.sciencedirect.com/science/article/pii/S0272884217325932.

[74] B. N. Peele, T. J. Wallin, H. Zhao, and R. F. Shepherd, "3d printing antagonistic systems of artificial muscle using projection stereolithography," *Bioinspiration & Biomimetics*, vol. 10, no. 5, p. 055 003, Sep. 2015. DOI: 10.1088/1748-3190/10/5/055003. [Online]. Available: https://doi.org/10.1088/1748-3190/10/5/055003.

[75] O. Carneiro, A. Silva, and R. Gomes, "Fused deposition modeling with polypropylene," *Materials & Design*, vol. 83, pp. 768–776, 2015, ISSN: 0264-1275. DOI: https://doi.org/10.1016/j.matdes.2015.06.053. [Online]. Available: http://www.sciencedirect.com/science/article/pii/S0264127515004037.

[76] Z. Weng, J. Wang, T. Senthil, and L. Wu, "Mechanical and thermal properties of abs/montmorillonite nanocomposites for fused deposi-

tion modeling 3d printing," *Materials & Design*, vol. 102, pp. 276–283, 2016, ISSN: 0264-1275. DOI: https://doi.org/10.1016/j.matdes.2016.04.045. [Online]. Available: http://www.sciencedirect.com/science/article/pii/S0264127516305196.

[77] H. Xin and M. Liang, "3-d-printed microwave and thz devices using polymer jetting techniques," *Proceedings of the IEEE*, vol. 105, no. 4, pp. 737–755, 2017. DOI: 10.1109/JPROC.2016.2621118.

[78] E. MacDonald and R. Wicker, "Multiprocess 3d printing for increasing component functionality," *Science*, vol. 353, no. 6307, 2016, ISSN: 0036-8075. DOI: 10.1126/science.aaf2093. eprint: https://science.sciencemag.org/content/353/6307/aaf2093.full.pdf. [Online]. Available: https://science.sciencemag.org/content/353/6307/aaf2093.

[79] L. E. Murr, S. M. Gaytan, D. A. Ramirez, E. Martinez, J. Hernandez, K. N. Amato, P. W. Shindo, F. R. Medina, and R. B. Wicker, "Metal fabrication by additive manufacturing using laser and electron beam melting technologies," *Journal of Materials Science & Technology*, vol. 28, no. 1, pp. 1–14, 2012, ISSN: 1005-0302. DOI: https://doi.org/10.1016/S1005-0302(12)60016-4. [Online]. Available: http://www.sciencedirect.com/science/article/pii/S1005030212600164.

[80] P. Wang, W. J. Sin, M. L. S. Nai, and J. Wei, "Effects of processing parameters on surface roughness of additive manufactured ti-6al-4v via electron beam melting," *Materials*, vol. 10, no. 10, 2017, ISSN:

1996-1944. DOI: 10.3390/ma10101121. [Online]. Available: https://www.mdpi.com/1996-1944/10/10/1121.

[81] J. Wang, A. Goyanes, S. Gaisford, and A. W. Basit, "Stereolithographic (sla) 3d printing of oral modified-release dosage forms," *International Journal of Pharmaceutics*, vol. 503, no. 1, pp. 207–212, 2016, ISSN: 0378-5173. DOI: https://doi.org/10.1016/j.ijpharm.2016.03.016. [Online]. Available: http://www.sciencedirect.com/science/article/pii/S0378517316302150.

[82] L. E. Murr, "Frontiers of 3d printing/additive manufacturing: From human organs to aircraft fabrication†," *Journal of Materials Science & Technology*, vol. 32, no. 10, pp. 987–995, 2016, ISSN: 1005-0302. DOI: https://doi.org/10.1016/j.jmst.2016.08.011. [Online]. Available: http://www.sciencedirect.com/science/article/pii/S1005030216301335.

[83] M. Too, K. Leong, C. Chua, Z. Du, S. Yang, C. Cheah, and S. Ho, "Investigation of 3d non-random porous structures by fused deposition modelling," *The International Journal of Advanced Manufacturing Technology*, vol. 19, Feb. 2002. DOI: 10.1007/s001700200016. [Online]. Available: https://doi.org/10.1007/s001700200016.

[84] S. Daminabo, S. Goel, S. Grammatikos, H. Nezhad, and V. Thakur, "Fused deposition modeling-based additive manufacturing (3d printing): Techniques for polymer material systems," *Materials Today Chemistry*, vol. 16, p. 100 248, 2020, ISSN: 2468-5194. DOI: https://doi.

org/10.1016/j.mtchem.2020.100248. [Online]. Available: http://www.sciencedirect.com/science/article/pii/S2468519420300082.

[85] G. I. Salentijn, P. E. Oomen, M. Grajewski, and E. Verpoorte, "Fused deposition modeling 3d printing for (bio)analytical device fabrication: Procedures, materials, and applications," *Analytical Chemistry*, vol. 89, no. 13, pp. 7053–7061, 2017, PMID: 28628294. DOI: 10.1021/acs.analchem.7b00828. eprint: https://doi.org/10.1021/acs.analchem.7b00828. [Online]. Available: https://doi.org/10.1021/acs.analchem.7b00828.

[86] T. Femmer, A. Jans, R. Eswein, N. Anwar, M. Moeller, M. Wessling, and A. J. Kuehne, "High-throughput generation of emulsions and microgels in parallelized microfluidic drop-makers prepared by rapid prototyping," *ACS Applied Materials & Interfaces*, vol. 7, no. 23, pp. 12 635–12 638, 2015, PMID: 26040198. DOI: 10.1021/acsami.5b03969. eprint: https://doi.org/10.1021/acsami.5b03969. [Online]. Available: https://doi.org/10.1021/acsami.5b03969.

[87] G. I., C. L.K., C. S.P., C. W. B. S.L., S. M., and L. S.H., "The use of rapid prototyping to assist medical applications," *Rapid Prototyping Journal*, vol. 12, Jan. 2006. DOI: 10.1108/13552540610637273. [Online]. Available: https://doi.org/10.1108/13552540610637273.

[88] A. Nuseir, M. M. Hatamleh, A. Alnazzawi, M. Al-Rabab'ah, B. Kamel, and E. Jaradat, "Direct 3d printing of flexible nasal prosthesis: Optimized digital workflow from scan to fit," *Journal of Prosthodontics*, vol. 28, no. 1, pp. 10–14, 2019. DOI: https://doi.org/10.1111/

jopr.13001. eprint: https://onlinelibrary.wiley.com/doi/pdf/10.1111/jopr.13001. [Online]. Available: https://onlinelibrary.wiley.com/doi/abs/10.1111/jopr.13001.

[89] H. Elayan, O. Amin, R. M. Shubair, and M. Alouini, "Terahertz communication: The opportunities of wireless technology beyond 5g," in *2018 International Conference on Advanced Communication Technologies and Networking (CommNet)*, 2018, pp. 1–5. DOI: 10.1109/COMMNET.2018.8360286.

[90] K. Huang and Z. Wang, "Terahertz terabit wireless communication," *IEEE Microwave Magazine*, vol. 12, no. 4, pp. 108–116, 2011. DOI: 10.1109/MMM.2011.940596.

[91] B. Scherger, M. Scheller, C. Jansen, M. Koch, and K. Wiesauer, "Terahertz lenses made by compression molding of micropowders," *Applied optics*, vol. 50, no. 15, pp. 2256–2262, 2011.

[92] A. Hernandez-Serrano, R. Mendis, K. S. Reichel, W. Zhang, E. Castro-Camus, and D. M. Mittleman, "Artificial dielectric stepped-refractive-index lens for the terahertz region," *Optics express*, vol. 26, no. 3, pp. 3702–3708, 2018.

[93] J. Liu, R. Mendis, and D. M. Mittleman, "A maxwell's fish eye lens for the terahertz region," *Applied Physics Letters*, vol. 103, no. 3, p. 031 104, 2013.

[94] S. Rana, A. S. Rakin, M. R. Hasan, M. S. Reza, R. Leonhardt, D. Abbott, and H. Subbaraman, "Low loss and flat dispersion kagome

photonic crystal fiber in the terahertz regime," *Optics Communications*, vol. 410, pp. 452–456, 2018.

[95] G. Kumar, S. Pandey, A. Cui, and A. Nahata, "Planar plasmonic terahertz waveguides based on periodically corrugated metal films," *New Journal of Physics*, vol. 13, no. 3, p. 033 024, 2011.

[96] N. Joshi and N. P. Pathak, "Tunable wavelength demultiplexer using modified graphene plasmonic split ring resonators for terahertz communication," *Photonics and Nanostructures-Fundamentals and Applications*, vol. 28, pp. 1–5, 2018.

[97] L. Jiu-Sheng, L. Han, and Z. Le, "Compact four-channel terahertz demultiplexer based on directional coupling photonic crystal," *Optics Communications*, vol. 350, pp. 248–251, 2015.

[98] S. Busch, M. Weidenbach, M. Fey, F. Schäfer, T. Probst, and M. Koch, "Optical properties of 3d printable plastics in the thz regime and their application for 3d printed thz optics," *Journal of Infrared, Millimeter, and Terahertz Waves*, vol. 35, no. 12, pp. 993–997, 2014.

[99] A. Squires and R. Lewis, "Mechanical and optical viability of eighteen filaments for 3d printing of terahertz components," in *Infrared, Millimeter, and Terahertz Waves (IRMMW-THz), 2017 42nd International Conference on*, IEEE, 2017, pp. 1–2.

[100] E. Castro-Camus, M. Koch, and A. I. Hernandez-Serrano, "Additive manufacture of photonic components for the terahertz band," *Journal of Applied Physics*, vol. 127, no. 21, p. 210 901, 2020.

[101] J. Sun and F. Hu, "Three-dimensional printing technologies for terahertz applications: A review," *International Journal of RF and Microwave Computer-Aided Engineering*, vol. 30, no. 1, e21983, 2020. DOI: https://doi.org/10.1002/mmce.21983. eprint: https://onlinelibrary.wiley.com/doi/pdf/10.1002/mmce.21983. [Online]. Available: https://onlinelibrary.wiley.com/doi/abs/10.1002/mmce.21983.

[102] M. Weidenbach, D. Jahn, A. Rehn, S. F. Busch, F. Beltrán-Mejía, J. C. Balzer, and M. Koch, "3d printed dielectric rectangular waveguides, splitters and couplers for 120 ghz," *Opt. Express*, vol. 24, no. 25, pp. 28 968–28 976, Dec. 2016. DOI: 10.1364/OE.24.028968. [Online]. Available: http://www.opticsexpress.org/abstract.cfm?URI=oe-24-25-28968.

[103] A. L. S. Cruz, V. A. Serrão, C. L. Barbosa, M. A. R. Franco, C. M. B. Cordeiro, A. Argyros, and X. Tang, "3d printed hollow core fiber with negative curvature for terahertz applications," *Journal of Microwaves, Optoelectronics and Electromagnetic Applications (JMOe)*, vol. 14, SI–45 to SI, Aug. 2015. [Online]. Available: http://www.jmoe.org/index.php/jmoe/article/view/489.

[104] J. Li, K. Nallappan, H. Guerboukha, and M. Skorobogatiy, "3d printed hollow core terahertz bragg waveguides with defect layers for surface sensing applications," *Optics Express*, vol. 25, no. 4, pp. 4126–4144, 2017.

[105] G. Wu, Y. Zeng, K. F. Chan, S. Qu, and C. H. Chan, "3-d printed terahertz lens with circularly polarized focused near field," in *2019 13th European Conference on Antennas and Propagation (EuCAP)*, 2019, pp. 1–4.

[106] M. Liang, J. Wu, X. Yu, and H. Xin, "3d printing technology for rf and thz antennas," 2016, pp. 536–537.

[107] M. Ahmadloo and P. Mousavi, "Application of novel integrated dielectric and conductive ink 3d printing technique for fabrication of conical spiral antennas," in *2013 IEEE Antennas and Propagation Society International Symposium (APSURSI)*, 2013, pp. 780–781. DOI: 10.1109/APS.2013.6711049.

[108] R. C. Rumpf, M. Gates, C. L. Kozikowski, and W. A. Davis, "Guided-mode resonance filter compensated to operate on a curved surface," *Progress In Electromagnetics Research*, vol. 40, pp. 93–103, 2013.

[109] D. Pan, H. Wei, and H. Xu, "Optical interferometric logic gates based on metal slot waveguide network realizing whole fundamental logic operations," *Opt. Express*, vol. 21, no. 8, pp. 9556–9562, Apr. 2013. DOI: 10.1364/OE.21.009556. [Online]. Available: http://www.opticsexpress.org/abstract.cfm?URI=oe-21-8-9556.

[110] P. Sharma and V. D. Kumar, "All optical logic gates using hybrid metal insulator metal plasmonic waveguide," *IEEE Photonics Technology Letters*, vol. 30, no. 10, pp. 959–962, 2018. DOI: 10.1109/LPT.2018.2826051.

[111] M. Moradi, M. Danaie, and A. A. Orouji, "Design of all-optical xor and xnor logic gates based on fano resonance in plasmonic ring resonators," *Optical and Quantum Electronics*, vol. 51, 2019. DOI: 10.1007/s11082-019-1874-0.

[112] L. He, W. X. Zhang, and X. D. Zhang, "Topological all-optical logic gates based on two-dimensional photonic crystals," *Opt. Express*, vol. 27, no. 18, pp. 25 841–25 859, Sep. 2019. DOI: 10.1364/OE.27.025841. [Online]. Available: http://www.opticsexpress.org/abstract.cfm?URI=oe-27-18-25841.

[113] Y. Liu, F. Qin, Z.-M. Meng, F. Zhou, Q.-H. Mao, and Z.-Y. Li, "All-optical logic gates based on two-dimensional low-refractive-index nonlinear photonic crystal slabs," *Opt. Express*, vol. 19, no. 3, pp. 1945–1953, Jan. 2011. DOI: 10.1364/OE.19.001945. [Online]. Available: http://www.opticsexpress.org/abstract.cfm?URI=oe-19-3-1945.

[114] R. Ge, B. Yan, J. Xie, E. Liu, W. Tan, and J. Liu, "Logic gates based on edge states in gyromagnetic photonic crystal," *Journal of Magnetism and Magnetic Materials*, vol. 500, p. 166 367, 2020, ISSN: 0304-8853. DOI: https://doi.org/10.1016/j.jmmm.2019.166367. [Online]. Available: https://www.sciencedirect.com/science/article/pii/S0304885318341660.

[115] W. Su and Z. Geng, "Terahertz all-optical logic gates based on a graphene nanoribbon rectangular ring resonator," *IEEE Photonics*

Journal, vol. 10, no. 6, pp. 1–8, 2018. DOI: 10.1109/JPHOT.2018.2874507.

[116] A. F. Aguiar, D. M. de C. Neves, and J. B. R. Silva, "All-optical logic gates devices based on spp coupling between graphene sheets," *Journal of Microwaves, Optoelectronics and Electromagnetic Applications (JMOe)*, vol. 17, no. 2, pp. 208–216, Sep. 2018. DOI: 10.1590/2179-10742018v17i21186. [Online]. Available: http://www.jmoe.org/index.php/jmoe/article/view/668.

[117] X. Zhang, J. Xu, J. Dong, and D. Huang, "All-optical logic gates based on semiconductor optical amplifiers and tunable filters," in *Optical SuperComputing*, S. Dolev and M. Oltean, Eds., Berlin, Heidelberg: Springer Berlin Heidelberg, 2009, pp. 19–29, ISBN: 978-3-642-10442-8.

[118] G. Berrettini, A. Simi, A. Malacarne, A. Bogoni, and L. Poti, "Ultrafast integrable and reconfigurable xnor, and, nor, and not photonic logic gate," *IEEE Photonics Technology Letters*, vol. 18, no. 8, pp. 917–919, 2006. DOI: 10.1109/LPT.2006.873570.

[119] M. Manjappa, P. Pitchappa, N. Singh, N. Wang, N. I. Zheludev, and R. Lee Chengkuo andSingh, "Reconfigurable mems fano metasurfaces with multiple-input–output states for logic operations at terahertz frequencies," *Nature Communications*, vol. 9, 2018. DOI: 10.1038/s41467-018-06360-5.